2019

Surfactant-Enhanced Size-Excluded Transport of Bacteria in Unsaturated Porous Media

Jialan Zhu
Lehigh University

Surfactant-Enhanced Size-Excluded Transport of Bacteria in Unsaturated Porous Media

by

Jialan Zhu

A Dissertation

Presented to the Graduate and Research Committee

of Lehigh University

in Candidacy for the Degree of

Doctor of Philosophy

in

Civil Engineering

Lehigh University

May 2019

Approved and recommended for acceptance as a dissertation in partial fulfillment of the requirements for the degree of Doctor of Philosophy

Jialan Zhu
"Surfactant-Enhanced Size-Excluded Transport of Bacteria Through Unsaturated Porous Media."

_____
Defense Date

_____
Gerard Lennon
(Dissertation Director)

_____
Approved Date

Committee Members:

_____
Dr. Derick Brown

_____
Dr. Tara Troy

_____
Dr. Steve Peters

Table of Contents

List of Tables

List of Figures

Abstract

This study investigated surfactant-enhance bacteria transport in variably saturated zone. Bacteria transport experiment results suggested that *Escherichia coli* K-12 (*E. coli*) travelled faster and are less likely to be retained when they are transported by surfactant solution. Anionic surfactant (linear alkylbenzene sulfonate) has a stronger impact than nonionic surfactants ($C_{12}E_4$ and $C_{12}E_{23}$) on enhancing *E. coli* transport. And the impact is amplified as surfactants concentration increased for all types of surfactants.

Numerical model was developed to simulate surfactant-enhanced bacteria transport phenomenon. Hydraulic model was based on the variably saturated sand column on which bacteria transport experiment conducted. The model consisted Richards equation, van Genuchten retention function, and Mualem unsaturated conductivity function. Hydraulic model simulated water content distribution in the sand column at steady state. The water content increased as a "S" shape along the depth from about 0.08 to 0.40 which indicated an excellent variably saturated condition. An advection-dispersion equation with one kinetic sorption site and size exclusion coefficient was proposed to account for surfactant-enhanced bacteria transport in the variably saturated condition. Model simulated *E. coli* breakthrough curves fit laboratory observed data fairly well (goodness of fit coefficient r^2 above 0.9) for all types of surfactants at all concentrations. Sensitivity tests deposition rate coefficient (k) and size exclusion coefficient (θ_{im}) indicated that θ_{im} is only parameter controlling the bacteria early breakthrough in the model which might indicate the significance of size exclusion effect in this study. Value of θ_{im} increased for all three surfactants with increasing concentration. While θ_{im} for anionic surfactant is significantly higher than that for nonionic surfactants. k presented

descending trend as LAS concentration increased. But it remained relatively constant for both nonionic surfactants. Calculations revealed that presence of surfactants increased the critical pore radius (r_c) of size exclusion effect which indicated more pores were excluded from bacteria. r_c was enlarged when surfactant concentration was increased. The maximum rc in presence of anionic surfactant was found to be 0.0045 cm, which was larger than that of nonionic surfactant 0.004 cm. This might due to negatively charged anionic surfactant increased electrostatic repulsion between bacteria and interfaces.

1. Introduction

1.1. Problem Statement

Understanding fate and transport processes affecting colloids in the vadose zone, also called the unsaturated or partly saturated zone, is essential for protecting groundwater and designing remediation systems. Approximately one trillion gallons of wastewater carrying contaminants, pathogens and other colloids is released from on-site wastewater treatment systems (OSWTS), as is shown in ***Figure 1-1***, to the subsurface in the U.S. each year [1]. This domestic wastewater travels down through the vadose zone until it reaches the water table, which is the upper limit of saturation in an unconfined aquifer. A properly functioning OSWTS retains and eliminates microbial contaminants before the waste water reaches the water table. However, a considerable number of malfunctioning OSWTS have led to widespread groundwater contamination and waterborne diseases outbreaks when significant amounts of contaminants and pathogens migrate down and reach the saturated groundwater [2], [3].

One key aspect of the domestic wastewater released into subsurface is that it contains surfactants, which are substances with both hydrophobic and hydrophilic properties. They have the ability to alter the surface or interfacial energies of surfaces by adsorbing onto them [4]. This ability makes surfactants very useful in industrial applications and domestic goodssuch as detergents, soaps, shampoos, and cleaners [5]. It was estimated that 7.7 billion pounds of surfactants are used as household cleaning detergent each year [6]. These tremendous quantities of surfactants-containing consumer products usage make domestic wastewater rich in surfactants. For example, a commonly used anionic

surfactant, linear alkylbenzene sulfonate (LAS), was found in the gray water discharged from washing machines in concentrations of 150 to 600 mg/L [7]. While surfactants themselves can be considered as pollution, their impact on pathogenic organism movement in porous medium is drawing increasing attention. A body of studies show that the presence of surfactants has two effects: it alters colloidal particles deposition mechanisms and enhances their transport through mediumthe subsurface environment. The resulting large colloids travel faster and further than predicted by typical approaches [8]–[18]. This factor is likely to be one reason that OSWTS fail so frequently. This effect accelerates the transport of microorganism in the subsurface which are possible explanations for the phenomenon.

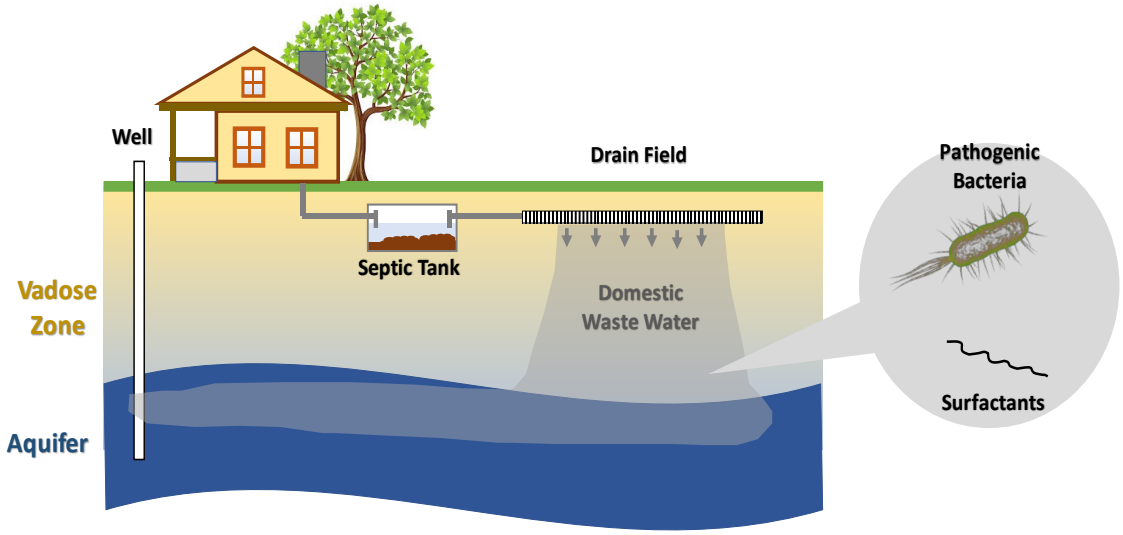

Figure 1-1. Schematic of on-site wastewater treatment systems (OSWTS). Domestic wastewater is stored in septic tank and released from drain field to the subsurface. The released domestic water contains pathogenic bacteria and surfactants which is a major source for groundwater contamination and outbreak of water borne diseases.

1.2. Overview of Bacteria Transport Models

Researchers have developed a number of models describing colloidal processes in unsaturated conditions in both porous medium, such as sand, and fractured rock. The discussion here focuses on porous medium. For example, colloid filtration theory (CFT) based on DLVO (Derjaguin-Landau-Verwey-Overbeek theory) forces has been used to characterize colloid deposition in the vadose zone [19]. Because the theory did not always match observations, researchers were motivated to develop models of other significant physical or chemical mechanisms, such as straining to explain high levels of observed deposition [19], [20]. Another significant process of colloidal transport in porous medium is size exclusion [17]. Size exclusion is the phenomenon that explains why colloids are more concentrated in the larger pore networks and have a higher average velocity as the colloids travel with the faster moving water. [21]. This generally results in an earlier colloid breakthrough and a higher microbe breakthrough concentration. Laboratory experiments demonstrated that relative size of pore throats and colloids (T/C) ratio influent the occurrence of size exclusion. And the size exclusion threshold T/C was found to be approximately 1.5 rather than the expected value of 1.0, since the colloids preferentially enter larger pores where direct flow prevails. [17]. Electrostatic forces also noticeably affect the distribution of colloid in porous medium. Anionic colloids tend to be excluded from the locations adjacent to negatively charged surfaces [22]. This leads to a stronger size exclusion for anionic colloids. As a result of size exclusion effect, the breakthrough of colloids is faster than conservative tracers [23], [24]. Moreover, the presence of an air-water interface (AWI) in the vadose zone plays an important role in

colloidal transport and deposition [25]. Colloids are preferentially sorbed onto AWI compared to other interfaces in porous medium, predominantly the soild-water interface (SWI) [26]. Schafer's bacteria transport study showed that the retention of bacteria dramatically increased with decreasing saturation in porous medium [27]. Although the surfactant effects on colloidal and bacterial transport in the vadose zone has not been extensively studied, researchers concluded that surfactants gather at the interfaces in porous medium, which then changes their interfacial properties and greatly affects colloidal deposition and size exclusion effects. Also, surfactants decrease the water surface tension, which results in a higher water velocity [27]–[32].

Numerical models accounting for microbial and colloidal transport in the vadose zone were developed based on current knowledge. Though the form of the model equations appears to show a great variety, they are based on the convection-dispersion equation with extension terms to describe additional processes such as reactions. For example, traditional models of colloid deposition have assumed a constant first-order sink term [19], [20], [24], [33]–[36]. Several approaches have been proposed to explain size-exclusion enhanced colloid velocity [20], [21]. The enhanced velocity effect is typically interpreted by (1) replacing the volumetric water content by a colloid accessible volumetric water content and (2) volumetric water flux by colloid accessible volumetric water flux in the convection-dispersion equation [19], [20]. Size exclusion also has noticeable implication on colloid attachment because the surface area accessible for attachment is decreased by confining colloid in large pores [21], [37]. However, the potential influence of this decreased surface area has not been fully studied.

1.3. Research Object and Approach

The objects of this study are to (1) numerically investigate surfactant-enhanced bacteria transport in an unsaturated sand column based on laboratory data and (2) elucidate the mechanisms behind the surfactant influences by analyzing numerical model results. Anionic surfactant (LAS) and nonionic surfactant (Brij 30 and Brij 35) were investigated in this study. The experiments focused on two influences of increased surfactant concentration: decreasing bacterial breakthrough time and increasing the bacterial breakthrough concentration. The experiments were conducted in a vertical 24-cm long sand column with steady surfactant solute passing through it and *Escherichia coli* K-12 (ATCC 29181) breakthrough data collected at the. A finite element numerical model was used to simulate the experimental conditions and predict the breakthrough data. The model was successfully fit to the observed data and provided an alternate way of exploring the surfactants' influence in the vadose zone. The relationships between the *E. coli* deposition rate coefficient, size exclusion factor and LAS concentration were the first time the surfactant influence was quantified in a numerical way. This dissertation also provides a systematic method for studying a comprehensive model which can be applied to more surfactants and conditions.

A detailed experimental description and model formulation of the surfactant-enhanced bacteria transport in the vadose zone is given in the first part of this dissertation (Ch.2 and Ch.3). Chapter 2 focuses on the unsaturated hydraulic condition while Chapter 3 addresses the surfactant-enhanced bacteria transport. The second part (Ch. 4) that

provides the mechanisms analysis based on the model result, which emphasizes on the surfactant impact on size exclusion effect.

Chapter 2 listed all the elements needed for building an unsaturated hydraulic model. Its object is to how numerical model guide the experiments. Separate experiments to determine parameters were conducted for porosity, hydraulic conductivity, and retention curves. The unsaturated Richards equation is discussed, and van Genuchten model was selected for the retention relationship with an excellent fit to the observed retention curve. The experimental data did not include the lower boundary condition, which was estimated by manually adjusting the water content distribution to match the observed points located 7 and 17 cm above the bottom of Ottawa sand.

Chapter 3 examined current colloid transport models with a wide array of options for modeling processes and presented the best-fit one for several types of surfactant and concentrations. The advection-dispersion equation is modified to include one kinetic deposition site and size exclusion coefficient provided an excellent correspondence between optimized and measured breakthrough curves. The Bromide test result was discussed in this chapter. It indicated that surfactants didn't show noticeable influence on flow pattern in the sand column. Hence, it was assumed the same pore-water velocity and bacteria dispersion coefficient for all transport experiments.

Chapter 4 underlines the significance of size exclusion in surfactant-enhanced bacteria transport. Comparison was drawn between a classical colloid filtration theory model, which doesn't consider size exclusion, and one modified with size exclusion coefficient. The results indicate that goodness of fit was significantly improved by including size exclusion. The hypothesis that deposition and size exclusion are the two main processes

accounting for the surfactant effects was confirmed by the model. Additionally, a hypothesis demonstration on surfactants' impact on them was made. More importantly, the relationship between the controlling parameters and surfactant concentration was investigated to reveal concentration effects on deposition and size exclusion processes. Furthermore, this chapter explored the pore size excluded from bacteria based on the size exclusion coefficient. The presence of surfactant was found dramatically increase the ratio of pore throat (the effective diameter of the pore) to bacteria diameter (T/C ratio), or the chance of size exclusion occurrence.

Finally, Ch. 5 provides the overall results and contributions of this study. The flaws of the model were highlighted along with the recommendations for future work.

2. Hydraulic Model of Variably Saturated Sand Column

2.1.Summary

Hydraulic model is the base of studying bacteria transport in variably saturated zone. A numerical hydraulic model usually consists of water flow equation, retention relationship equation, and unsaturated hydraulic conductivity equation. Each of them require a series of hydraulic information which is able to be obtained from either direct laboratory experiments measurement or indirect parametric estimation approach.

Richards equation coupled with van Genuchten retention model and Mualem hydraulic conductivity model is suitable for simulating sand column in this study. Independent laboratory experiments for the required hydraulic information were designed including porosity test, saturated hydraulic conductivity test, and retention relationship test. van Genuchten parameter α and *n* were estimated using optimization approach. The excellent model fit with observed retention curve indicates reliable van Genuchten parameter set. HYDRUS 1D finite element code was adopted to solve the equations. The hydraulic model was run until water flow reached steady state. The water content distribution at steady state was achieved which provided an insight of the flow characteristic within the sand column and was necessary for studying bacteria transport.

2.2.Introduction

The numerical hydraulic model includes the equations and boundary conditions describing the water system, and the finite element method applied to discretize the equations. As for surfactant-enhanced bacteria transport in the vadose zone phenomenon in this study, the hydraulic model is expected to account for the unsaturated water flow infiltration.

The vadose zone is generally defined as the geologic region below land surface and above groundwater table [38]. The key aspect of it is that soils and bedrock in this region are usually unsaturated whereas it is saturate below the water table (and an capillary zone just above the water table). That is, all three phases (solid, liquid, and gas) coexist in vadose zone; the gas zone can be just air, or include volatilized compounds. The presence of gas dramatically increases the complexity of vadose zone problems compared to normal saturated groundwater problems. Volumetric water content θ [length^3/length^3] is an important quantity for almost all vadose zone, and is the ratio of volume of water to the volume to the total volume in a sample of the porous medium [39], [40].

Those pores in nature display complex structures due to variable shape, size, and arrangement of the solid grains. It is not possible to obtain these information in most occasions. Pore structure models were developed and they may be divided into two categories. Models in first category simplify grains in porous medium as arrays of spherical particles. They provide qualitative explanation for processes in porous medium such as hysteresis. However, they only applicable for relative simple grain arrangement, not ready for quantitative predictive purpose. The second category consist of the simplest

and most widely used models. They consider the pore structure as arrays of capillary tube which is usually referred to as bundle of capillary tubes model. Each capillary has a uniform diameter throughout the length. The pore space can be easily calculated as a function of capillary pressure [41]. But the intense simplification of pore structure may lead to discrepancy between model result and experimental observation.

Richards equation is the most widely used governing equation for variably saturated water flow and has a clear physical basis [42]. It is a nonlinear partial differential equation usually expressed in terms of two dependent variables, water content and capillary pressure head [40]. It is usually coupled with soil-water retention function to solve it numerically.

Soil-water retention, or soil moisture characteristic, is the relationship between the volumetric water content θ [length^3/length^3] and matric potential (or capillary pressure head h, [length]) is called the retention curve [43]. It is a very important characteristic for soil under unsaturated conditions, and a number of researchers have developed equations to describe this relationship. The most famous van Genuchten model is the one used in this dissertation [44]. This model introduces four parameters, some of whichwere directly measured in the laboratory. Others were obtained by fitting the equation to an observed retention curve using parameter optimization technique. Parameter optimization is an indirect approach for estimating model parameters which are difficult to obtain in laboratory [45]. This approach was heavily used in this study.

Under unsaturated conditions, the value of hydraulic conductivity K [length/time] is highly variable and strongly dependent on saturation of the porous medium. When water content in a porous medium is below the residual water content, water cannot move

within it, and the value of K is 0. As the water saturation increases, water first fills enough of the pores for the water to move, and as it increase more, K increases. When the water content becomes saturated, K reaches its maximum value which is saturated hydraulic conductivity K_s [46]. Simple equations such as Gardner's equation and Campbell's equation consider K as a function of h or θ, often a power law [47]–[49]. Other advanced functions have been derived based on the pore-size distribution model of Burdine or Mualem in combination with retention functions [50], [51].

The laboratory sand column setup and research purpose determined the hydraulic models: unsaturated water flow model was 1-D mixed form Richards equation, the retention function was van Genuchten model, and unsaturated conductivity equation was Mualem function. Meanwhile conversely, the hydraulic models determined the hydraulic properties need to be obtained from experiments. A series of tests were conducted to fill the blank data required by the numerical model.

The main objective of this Chapter is to build hydraulic model based on the experimental hydraulic condition and figure out water flow characteristics in the sand column. Furthermore, it provides a list of hydraulic properties needed to complete a hydraulic model and an example on numerical model guiding experiments.

2.3. Laboratory Experiments

This section discussed hydraulic condition and properties tests of the unsaturated sand column which was designed by Tripathi and Brown. The sand column setup was outlined and additional tests on sand properties were provided.

2.3.1. Sand Column Experiments

The experiments of bacteria transport in the presence of surfactant conducted by Tripathi and Brown were simulated by the model developed in this dissertation. The experimental apparatus mainly consisted of a 25-cm sand column through which bacteria were transported. The experiment setup is briefly introduced in the first sections. Shweta's experimental work focused on bacteria breakthrough and did not include measurement of some essential hydraulic properties of the sand column which are essential for building hydraulic model. The next section discusses the additional experiments conducted as part of this research to identify missing parameter values using the same sand.

The primary goal of the sand column experiments is to mimic the vadose zone condition. However, the high complexity and variability of the natural vadose zone could affect the goal of studying surfactant effect on bacteria transport in this study. To achieve the primary goal, the sand column was designed in a greatly simplified lab scale to eliminate as many disturbances as possible. The simplifications include:

1. The water flow entering through the sand column is spread uniformly across the top to minimize preferential flow;
2. Maintaining steady water flow to avoid time-dependent variables;

3. Minimizing the saturated capillary fringe formation, so that the bacteria transport within essentially represent transport in unsaturated porous medium. In the natural environment, the capillary from is predicted to be more than the 25 cm height of the experimental column.

As show in ***Figure 2-1.*** *Schematic of the column experiment setupError! Reference source not found.*, the main experiment apparatus consisted of a 30-cm tall sand column assembly, two peristaltic pumps (Masterflex, Cole Parmer) installed at inflow and out flow end of the column, and two theta moisture probes (type ML2x, Dynamax Inc) installed at 8 cm and 18 cm from the bottom of the column.

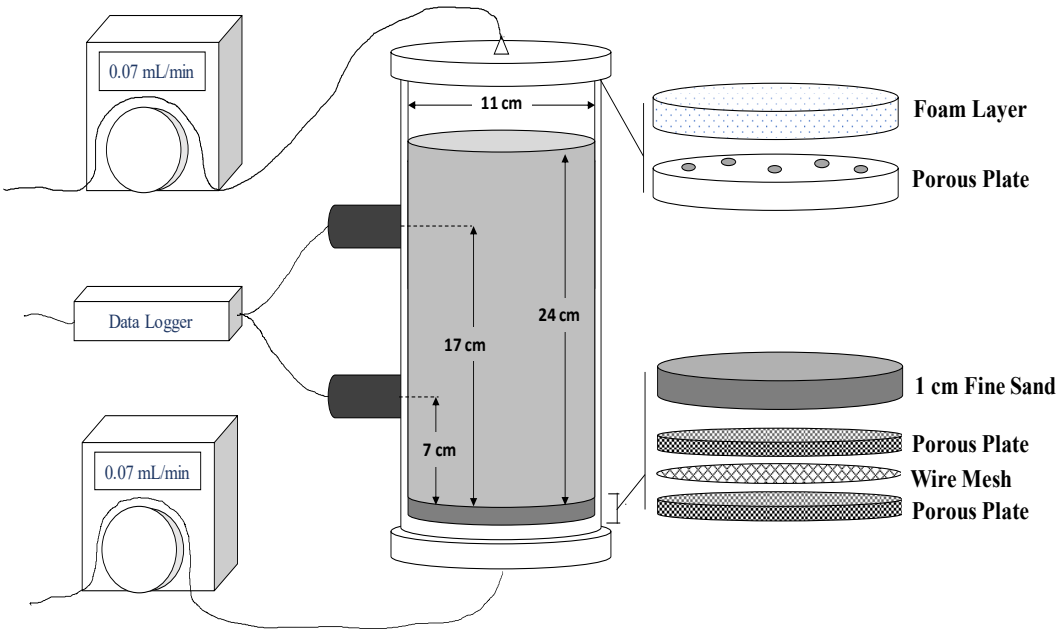

Figure 2-1. Schematic of the column experiment setup

The column was made of clear Poly-Vinyl Chloride (PVC) material. Clean water or experimental solutions were pumped into the column at the top (inflow) and out at the bottom (outflow) by the peristaltic pumps, carefully maintaining equal flow. A

hydrophilic polyurethane foam sheet (Rynel foams, Inc) and a plastic plate with twelve evenly distributed tiny holes were layered and placed at the top (inflow) of the column to help uniformly distribute the water drops over the cross-section area of the sand to reduce the chance of preferential flow occurring. Ottawa sand (ASF 50/70, US Silica) was packed in the column to a height of 24 cm. The sand was washed three times with deionized water (DI) to remove any fine particles prior to use. A wet packing technique was applied to provide a uniform and repeatable sand conditions which helped to evenly distribute water flow to achieve as close to uniform flow as possible. A 1-cm high fine sand (SIL-CO-SIL 125, US Silica) was packed at the bottom of the column right below the Ottawa sand pack to eliminate the formation of capillary fringe in the overlying Ottawa bulk sand. A finer wire mesh (pore size 55 μm) placed below the fine sand prevented it from being washed away. After wet packing, the column was drained by gradually adjusting inflow and outflow rate until a stable water moisture level (saturation) was achieved. The two moisture probes were used to monitor the moisture level in the laboratory column during the experiment. The minor variations in moisture level over time indicated the steady state of the water flow and repeatable water gradient within the column. A flow rate of 0.7 mL/min was found to be optimum for achieving steady water flow and used throughout all transport experiments.

At this flow rate, the top moisture probe reading was approximately 15% and the bottom one was approximately 65%.

2.3.2. Hydraulic Properties Tests

This section presents the hydraulic properties tests required by the hydraulic model that were conducted as part of this dissertation work. These experiments are:

1. porosity tests of the sands,
2. saturated hydraulic conductivity test,
3. test to define the retention curve

2.3.2.1. Porosity measurement

Porosity ϕ [length^3/length^3] of a porous medium is defined as the ratio of the void volume V_v [length^3], or pore space, to the total volume of the material V_t [length^3]: $\phi = V_v / V_t$ [39], [46].

Porosity of the coarse Ottawa sand (AFS 50/70, US Silica) and fine Berkeley Springs sand (SIL-CO-SIL 125, US Silica), were determined using the water evaporation method [52]. This method assumes that the volume of water retained in a saturated porous medium sample is equal to the volume of the void. The void volume can be estimated by measuring the amount of water in the saturated porous media. Sand was first immersed in DI water to make it saturated. The saturated sand was than packed into a 44 mL iron box to just fill the iron box so the volume v of the sample is also 44 mL. The iron box with saturated sand was weighed with an electronic balance, and the mass was recorded as m_s. After heating an hour in the oven to make sure that water in the sample has completely evaporated. Iron boxes containing the dried sand sample was reweighed and dry mass recorded as m_d. The mass of water in the original saturated sand sample can then be calculated by $m_w = m_s – md$, and the volume was obtained using $v_w = m_w / \rho$, where ρ is the density of the water [mass/length^3]. Assuming v_w was equal to the volume of the void in the porous medium, and with the total volume of the sample known to be 44 mL, the porosity is $\phi = v_w / 44$ mL. The procedure was repeated four times for each type of sand,

and the average of the four samples was used. The porosity of coarse Ottawa sand was found to be 0.40, and that of fine Berkeley Springs sand was 0.35.

2.3.2.2. Saturated Hydraulic Conductivity Measurement

Hydraulic conductivity K is a parameter introduced in Darcy's law, it describes the ease of water passing through a porous medium [46], and the saturated value is a key parameter for simulating partly saturated flow. One of the most commonly used laboratory methods to determine saturated hydraulic conductivity is the falling-head method [53], and was the technique used in this dissertation. It can be achieved with a laboratory apparatus commonly found in geotechnical and groundwater labs. ***Figure 2-2*****Error! Reference source not found.** shows the experiment setup of an iron tank with an open surface area of 750 cm^2 filled with water. The water surface in the tank was set as the reference level of hydraulic head equal to zero. A PVC column was placed just above the water surface with the bottom of the column in contact with the water surface. Hence, the hydraulic head at the column bottom section was assumed to be zero. Ottawa was packed to a depth of 20 cm in the PVC column prior to the experiment using a wet packing technique to minimize variation in the hydraulic conductivity due to the packing method. Full saturation of the Ottawa sand was ensured by an initial 4 cm depth of water above the sample and a removable plastic plate at the bottom. The initial height of the water surface in the column above the reference level (the water surface in the tank, y_0) was recorded. The experiment was started by removing the plastic plate, allowing gravity to cause the water in the column to flow down and out of the column. The height of water over time

was recorded (t), ending with the time it took for the water surface in the column to reach the top of the Ottawa sand surface, recorded as the water level at the top of the sand (y_t).

The principle of this method assumes the sand is saturated flow and flow is vertically downward. Hence, the instantaneous Darcy velocity v can be calculated using Darcy's law: $v = - K_s (\Delta y / \Delta L)$, where K_s is the hydraulic conductivity [length/time]; Δy is the hydraulic head difference between the Ottawa sand surface section and bottom section at that instant [length]. The column bottom in contact with the free surface in the tank so its head relative to the tank water level is zero. Because the section area (95 cm^2) is filled with sane and much smaller than that of tank (750 cm^2), the increase of water level in the tank due to water recharge from the column was negligible. Hence, Δy was always the instantaneous height of the water surface in the column above that in the tank in this experiment. L_s was the distant between the two sections which was the thickness of Ottawa sand (20 cm).

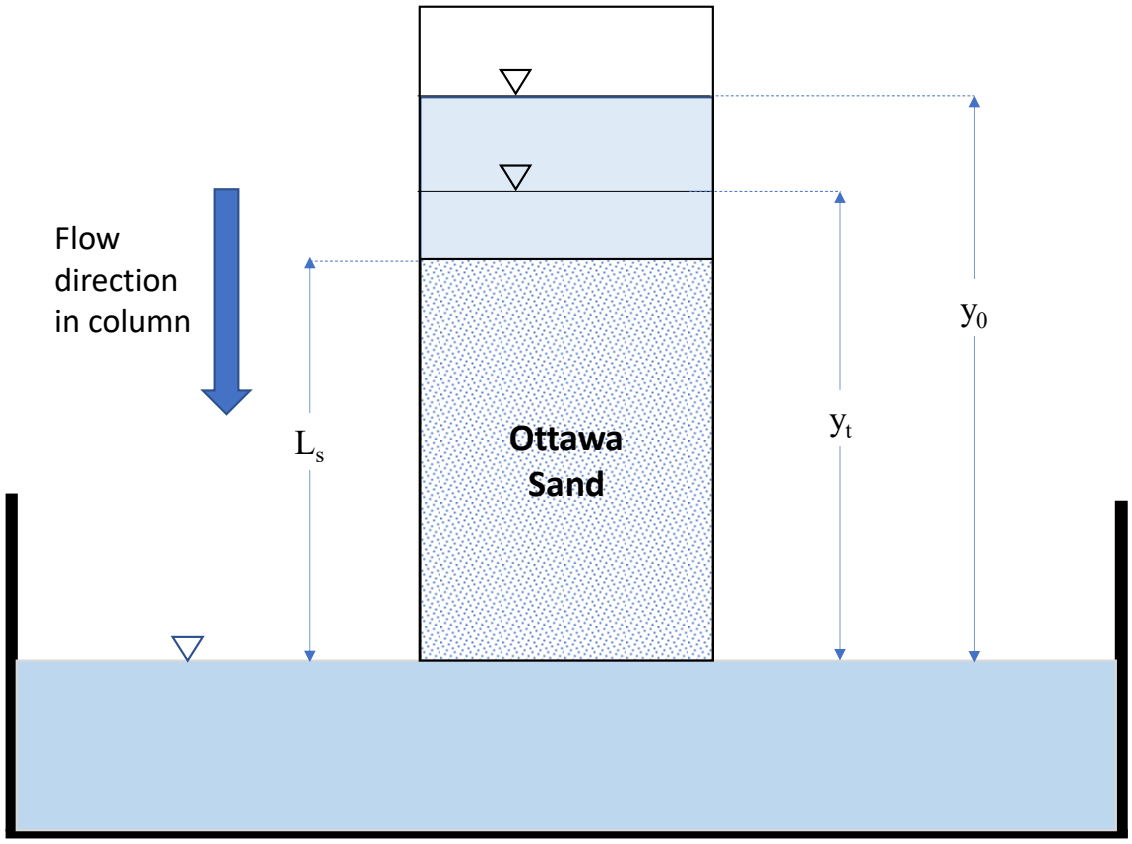

Figure 2-2. Schematic of saturated hydraulic conductivity test with falling-head method.

Combine Darcy's law with differential equation $v = \partial y/\partial t$ and integrate them from y_0 to y_t yielded the final form of hydraulic conductivity equation that takes the variable driving head difference into account [54]:

$$y = y_0 e^{-\frac{K}{L_s}t} \qquad \textbf{Equation 2-1}$$

The classical falling-head method selects two temporal points (t_1 and t_2) and their corresponding water level (y_1 and y_2) in the experiment to calculate K_s from Equation 2-1**Error! Reference source not found.** . Instead of calculating K from just two data points, the time and water level were recorded every 0.25 cm of water surface drop until

it reached sand surface. and the experiment was repeated three times. The data in Figure 2-3 represent the observed y *vs.* t data for each of three trials. Observed data was then fitted using

Equation ***2-1*** by trying different values of K until a 'best overall fit' was achieved. This modified falling-head method takes more data into consideration to avoid experimental errors to the degree possible and improve the accuracy of the K value. The solid line in Figure 2-3 is the fitted resulting best fit to all three trials for K_s of 0.054 cm/s (194 cm/hour) , with corresponding r^2 of 0.935. Thus a K_s of 194 cm/hour for Ottawa sand under Tripathi and Brown's laboratory condition was used in numerical model simulations of their column.

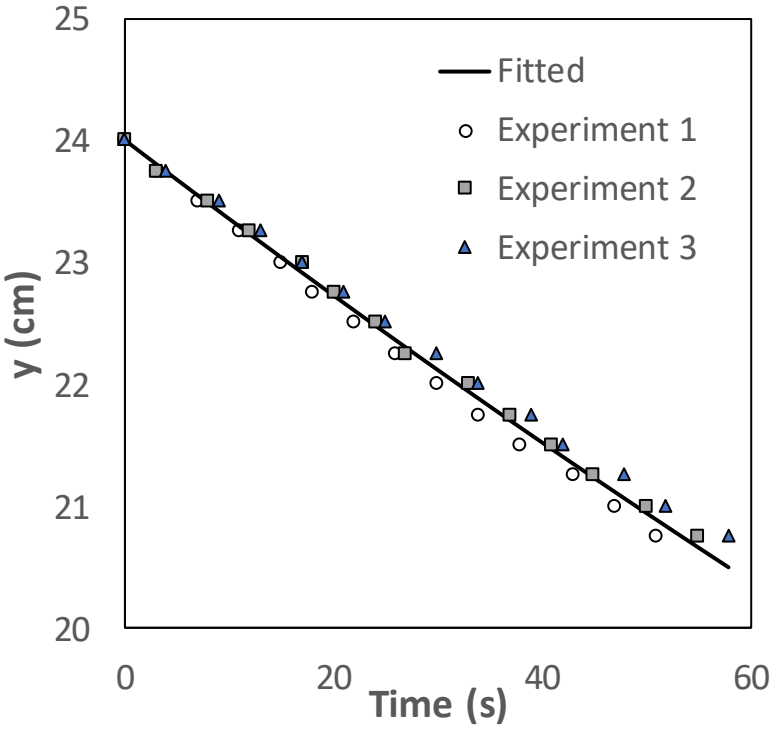

Figure 2-3. Result of matching theoretical falling-head with experimental observation. the various shapes of dots represent observed data from three duplicated tests. The solind line is the simulated falling-head with Equation 1.

2.3.2.3. Retention curve test

Soil water retention curves are generally developed by starting with a high water content and draining it to a low value, and are called drying curves or moisture release curves [40]. The retention curve was directly measured in the laboratory by draining saturated a sand column. As show in ***Figure 2-4***, a PVC column was filled with saturated Ottawa sand using the same packing method as for the bacteria transport experiments. One theta moisture probe (type ML2x, Dynamax Inc) was fully inserted into the Ottawa sand 18 cm above the bottom of the PVC column and connected to a data logger (type GP1, Delta T Inc) to record the soil moisture during the experiment. A pressure gauge (type 700G30, FLUKE Inc) was installed on the other side of the column at the same elevation as the moisture probe to record the corresponding pressures. The sensor cap of the pressure gauge was inserted in the sand region where was close to the needle sensor of the moisture probe. Hence, it was assumed that both moisture probe and pressure gauge measured the same point in the Ottawa sand. The water exiting the column bottom was collected with one peristaltic pump (Masterflex, Cole Parmer). Before the experiment, the readings of water saturation and capillary pressure from two moisture probe and pressure gauge were checked. The moisture content was equal to the porosity value of 0.40, and capillary pressure was approximately zero, both of which correspond to saturated conditions. The experiment began by starting the pump, which started drying out the column. Every time the moisture reading decreased about 0.01, the pumped was turned off for about 5 minutes until the readings in both gauges became stable and the moisture and pressure readings were recorded. Then the pump was turned on again and the

procedure was repeated until the soil moisture didn't change over a 30-minute drainage time, which indicated that water content in the sand column was close to the residual water content value.

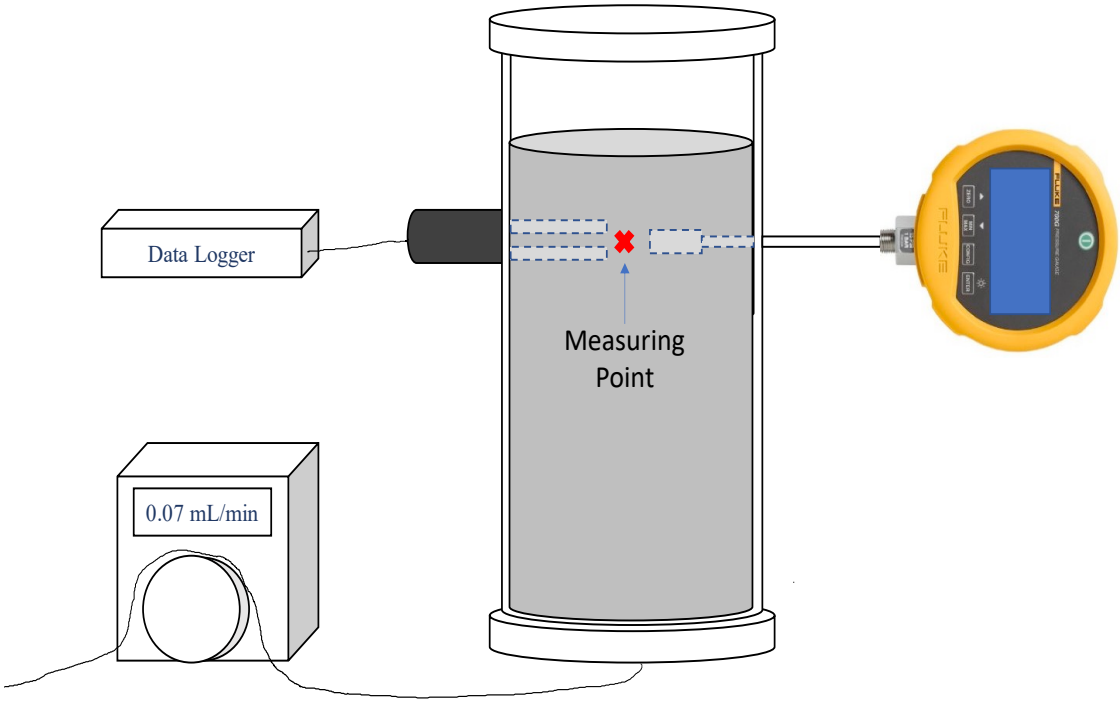

Figure 2-4. Schematic of retention curve test setup.

Figure 2-5 presents the measured retention points. The exception to the stated procedure was the initial reading, which changed dramatically, with the water content typically dropping from 0.4 (saturated) to 0.3 in less than 10 seconds. This increased the difficulty of measurement and collected data was relatively scattered (shown in red circle). After this stage, the decrease of water content became slower and steadier. More data were collected and water content showed an approximately linear relationship with capillary pressure. As the moisture in the sand continued decreasing, it became more and more difficult to drain water out of the column. When the water content was below 0.04, it

didn't change any more over 30 minutes period. Hence, 0.04 was assumed as the residual water content θ_r. The relationship between water content and capillary pressure from sand saturated to residual water content is the full shape of retention curve.

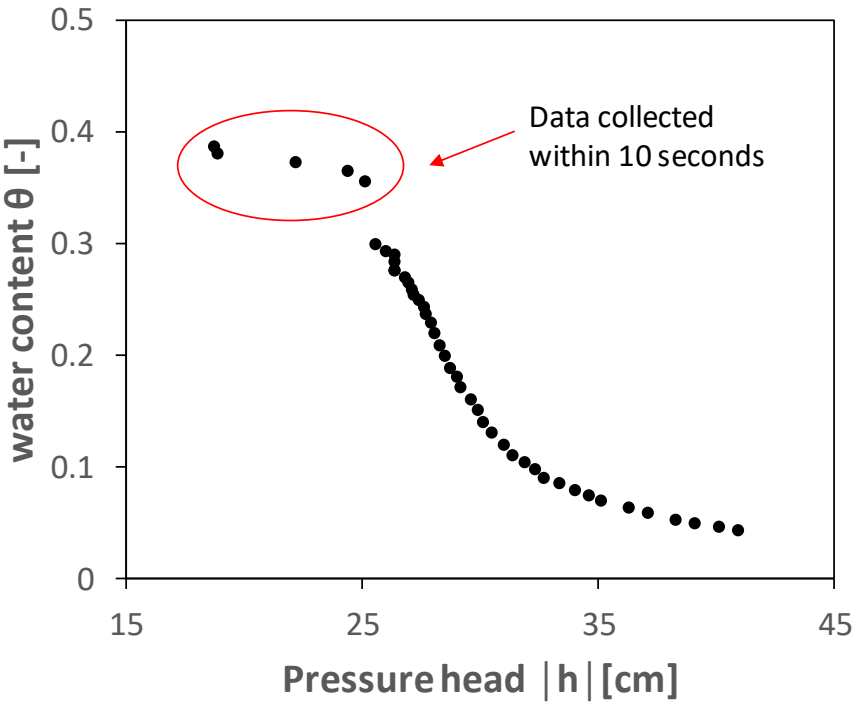

Figure 2-5. Result of retention curve test. Each dot represent a pair water content and capilllary pressure head measured at the same time and same location in the sand column. The data in the sand column were collected within ten seconds after experiment started when saturation changed dramatically.

2.4. Hydraulic Model

The hydraulic model of the sand column is an essential part of simulating bacteria transport. The Hydraulic model was applied to simulate the experimental flow condition within the sand column, providing information on flow rate, saturation distribution, and flow state, all of which greatly influent fate and transport of bacteria in unsaturated porous medium.

2.4.1. Governing equations

This section discussed governing equations in hydraulic model of unsaturated sand column. According the nature of the laboratory sand column, the 1D Richards equation combined with van the Genuchten model and Mualem model was selected in this study.

2.4.1.1. Richards Equation

Unlike a saturated groundwater model, the vadose zone hydraulic model is much more complicated due to the existence of the gas phase [55]. The degree of saturation in the vadose zone can change over time and space and typically below 100%. Therefore, saturated groundwater equations cannot be directly applied in vadose zone problems. Moisture (water) content (θ) is key quantity for understanding the water distribution (for unsaturated problems media and is used in virtually all studies or models of unsaturated zone including the classical Richards equation [39], [56]. Recall that the definition of water content is the ratio of water volume to total sample volume.

The water flow in this study was predominantly vertically downward with assumed evenly distributed infiltration. Hence, the one-dimensional Richards equation is expressed as:

$$\frac{\partial \theta}{\partial t} = \frac{\partial}{\partial x}\left[K\left(\frac{\partial h}{\partial x} + 1 \right) \right] \qquad \textbf{Equation 2-2}$$

where K is the unsaturated conductivity [length/time]; h is the capillary pressure head [length]; t is time; and x is the spatial coordinate [length] positive upwards. For 2D or 3D flow, the vertical coordinate is usually chosen as z. Equation 4 is called mixed-form because it has two-dependent varibles (θ and h); typically, K(h) has an unknown dependency on h usually determined experimentally.

2.4.1.2. van Genuchten Model

The variation of θ with h can be observed from discrete points of the experimental retention curve (as shown in ***Figure 2-5***). Each point represents a pair of θ and h values, with interpolated values between measured points. However, because the data does not follow a linear trend in either normal or log scale, the best way to interpolate values is fitting continuous parametric functions. Such functions are well behaved, have smoother derivatives (slopes) and cause fewer numerical problems, which is the main reason for being widely applied in numerical models [40], [57]. One of the most popular retention curve models is one developed by van Genuchten [44], [58], it is expressed as:

$$\theta(h) = \begin{cases} \theta_r + \dfrac{\theta_s - \theta_r}{\left[1 + \left|\alpha h\right|^n\right]^m} & h < 0 \\ \theta_s & h > 0 \end{cases}$$ **Equation 2-3**

where θ_r is the residual volumetric water content [length^3/length^3]; θ_s is saturated volumetric water content [length^3/length^3]; α [length^{-1}] is a parameter to scale the matric head; both n [-] and m [-] are fitting parameters. To eliminate one of the parameters, we adopted van Genuchten proposed relationship of m = 1 – 1/n, which still allows an excellent fit to the experimental data.

2.4.1.3. Unsaturated Conductivity Model

The relationship between K and saturation (or capillary pressure) is rather difficult to measure in the lab, and a hydraulic conductivity function derived from pore-size distribution model of Burdine (1953) and Mualem (1976) is often used [59]. Their models are based on considering the pore structure as a bundle of capillary tubes with different radius. But radius of each tube is uniform along the length. Equation 2-4 is Mualem hydraulic conductivity function.

$$K\left(S_e\right) = K_s S_e^l \frac{\left[\int_0^{S_e} \dfrac{dS_e}{h\left(S_e\right)}\right]^2}{\left[\int_0^1 \dfrac{dS_e}{h\left(S_e\right)}\right]^2}$$ **Equation 2-4**

where $S_e = (\theta - \theta_r) / (\theta_s - \theta_r)$ is the effective saturation [-]; K_s is the saturated hydraulic conductivity [LT^{-1}]; l is a pore-connectivity parameter [-], estimated to be approximately 0.5 for many soils; $h(S_e)$ is the water retention curve relationship [L].

When using van Genuchten relationship for $h(S_e)$, Equation 2-4 becomes:

$$K\left(S_e\right) = K_s S_e^l \left[1 - \left(1 - S_e^{1/m}\right)^m\right]^2 \qquad \textbf{Equation 2-5}$$

2.4.2. Parameter optimization

The shape of simulated retention curve is determined by these model parameters (l, m, Se and K_s). They are required prior to obtain the fitted functions to experimental data using the van Genuchten model. Although a variety of parameter sets can reasonably fit a soil water retention curve, using a parameter identification technique leads to a unique parameter set that best fits Tripathi's experimental conditions. Some of the parameters are not possible to acquire through direct laboratory method, such as parameter m, so following a common inverse method, the best set of parameters are identified that provides a best fit of the van Genuchten function curve to the observed retention curve data. This process is called parameter optimization.

Some discrepancy exists between the observe retention curve and van Genuchten function fitting curve because the smooth function curve does not go through every observed data point. First, it is not possible to fit all discrete data points with one simple continuous function; second, it is not necessary to do so since error exist in observed data due to laboratory measurement. The inverse method is based on minimizing this discrepancy to achieve a "best fit" [60], [61]. The goodness of fit, or the magnitude of the

discrepancy, is generally evaluated by objective function.

Equation ***2-6*** is the calculation based on a least squared differences objective function:

$$O(b)=\sum_{i=1}^{N}\left\{w_i\left[\theta_i-\hat{\theta}_i(b)\right]\right\}^2 \qquad \textbf{Equation 2-6}$$

where b is the set of parameter estimates. In this case, b consists of α and n from van Genuchten model Equation 2-3; N is the number of the retention data points; θ_i and θ_i are the observed and simulated water content, respectively; w_i is used to assign weight to each single data point, its value range is 0 ~ 1. The assigned value depends on the level of confidence in the data points. The retention data points collected within 10 seconds were assigned 0.9 weight. Because the water content decreased dramatically during this period, which may result in more measurement error. Weight of the rest of data points were 1.0. The calculation of best fit parameters was obtained by the RETC program, developed to fit a number of popular analytical soil water retention curve functions including van Genuchten model [40], [62]. The initial estimates of α and *n* used to calculate the objective function in Equation ***2-6***, are changed repeatedly, and the calculated objective function guides an iterative process to determine minimum value the least square objective function (

Equation ***2-6***), which identifies the best parameter set.

2.4.3. Numerical model

Equation 2-4 and Equation 2-5 were then coupled with Richards Equation (

Equation ***2-2***). The unknowns in Richards Equation were reduced from two dependent variables and an unknown parametric relationship for K, to a single dependent variable

(h) and known parametric relationship, which is more readily solved. The resulting single equation is a highly nonlinear function and analytical solution is difficult to achieve, so a numerical method is recommended. The HYDRUS-1D finite element code is an excellent choice [35], [62]. All the equations mentioned above are implemented in the code. And they are solved numerically using Galerkin-type linear finite element schemes.

2.4.3.1. Model Discretion and Initial Conditions

The 24-cm sand column was discretized into 25 evenly spaced nodes every 1-cm. ***Figure 2-6*** shows the model discretization concept. Red dots represent the nodes in the numerical model. Each node stores hydraulic information as a function of time at its specified location, such as water content, capillary pressure, and flow rate. The goal is to obtain these information at steady state. And the steady state information depends on hydraulic properties and boundary conditions rather than initial condition. The initial condition of the unknown dependent variable in

Equation ***2-2***is h. Arbitrary h could be used because steady state is independent with initial condition. The initial condition of h = 0 corresponds to being fully saturated at all internal nodes. after setup boundary conditions, the model was run until the water flow reached steady state. The model output is h value at all nodes, other hydraulic information such as water content is derived from the parametric relationships.

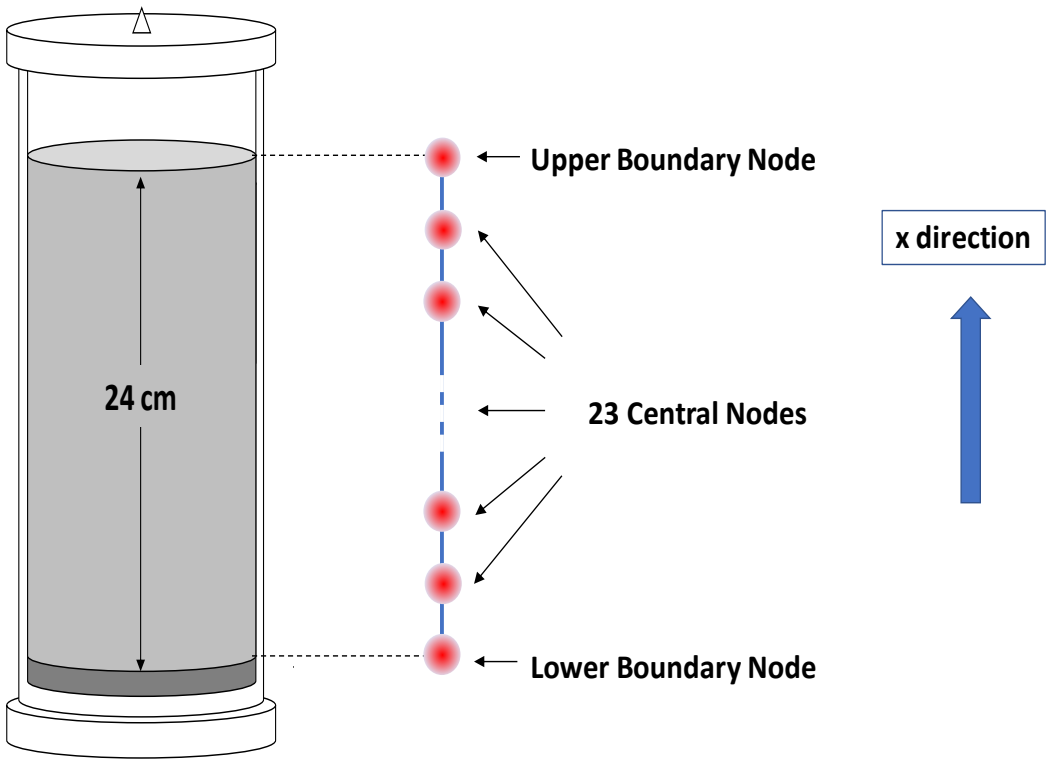

Figure 2-6. Schematic of model discretization. The red dots represent the nodes in the model. Water flow information is stored in these nodes. The blue arrow indicates that the positive direction is vertical upwards in this model.

2.4.3.2. Boundary conditions

The choice of boundary condition at the upper boundary includes specifying h, or its derivative or a mixed condition. Tripathi's flow rate was measure because the water or solution pumping rate was kept constant in the laboratory; dividing the flow rate by the top area, yielded a constant flux of q = 0.44 cm/hour. The HYDRUS-1D model allows the flux to be specified, from which it calculates a corresponding value of derivative of h However, the constant head lower boundary condition data, the capillary head at the bottom of the Ottawa sand, was missing. This essential data was acquired indirectly in this study. As mentioned in former sections, saturation at 8 cm and 18 cm above the bottom of PVC column were kept 65% and 15%, or 7 cm and 17 cm that of Ottawa sand

(minus 1-cm fine sand). Saturation 65% and 15% can be converted to capillary pressure head -26.0 cm and -34.0 cm using water content vs. capillary pressure head relationship (retention curve). The capillary pressure head increased with depth in the sand column because the saturation was increased with depth. The bottom boundary condition which has the greatest depth should have a larger head value than any other location in the sand column. Hence, the capillary pressure head at bottom must be a value between -26.0 cm and 0.0 cm. Guess and error method was used to locate the value. 260 bottom boundary condition candidates were created by spacing -26.0 to 0.0 with 0.1. Each of them was used in the model and the responding model results was compared with observed saturation. For example, the capillary pressure head was set constantly equal to -10 cm at the bottom node in the model to represent the constant head lower boundary condition. After calculating, the model yielded capillary pressure head distribution at all nodes. Then the model simulated head at 7 cm and 17 cm above the bottom with those of observed was compared. This procedure was repeated for all candidates. The one with the smallest discrepancy is the most possible head for lower boundary condition. It was found h = -20.2 cm provided the best fit. Result is shown in right side of ***Figure 2-9***. The black dot is the observed capillary pressure head at 7 cm and 17 cm above the Ottawa sand bottom. The solid line is the model simulated result with lower boundary condition h = -20.2 cm.

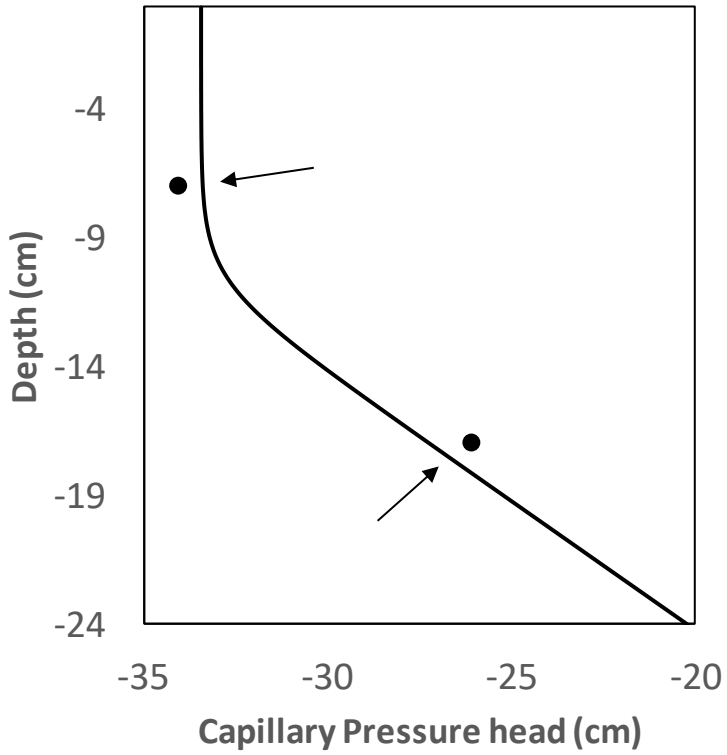

Figure 2-7. Result of matching capillary pressure profile with observed data. The two black dots represent known capillary pressure head at 7 cm and 17 cm above the bottom whicn are converted from observed moisture. The solid line is the model simulated capillary pressure head.

2.5. Results

2.5.1. Simulating retention curve

There are five parameters need to determine in van Genuchten model: θ_s, θ_r, α, n, and m. Both θ_s and θ_r were obtained from experiment. And m may be calculated through the m and n relationship: $m = 1 - 1/n$. Hence, only two parameters left (α and n) left to be obtained through parameter optimization method.

Figure 2-8 presents the result of model fitting observed retention curve. van Genuchten model works excellent on fitting the observed Ottawa sand retention curve. The red circles are observed retention data and the solid line is the fitting retention curve based on van Genuchten model. The goodness of fit r^2 is as high as 0.998 which indicates a very small discrepancy between observed data point and simulated curve. The parameter set (α = 0.04, n = 12.66) yielding this curve is the most possible van Genuchten parameter set for the Ottawa sand in this study. They were used to complete the retention curve function and also calculate unsaturated hydraulic conductivity.

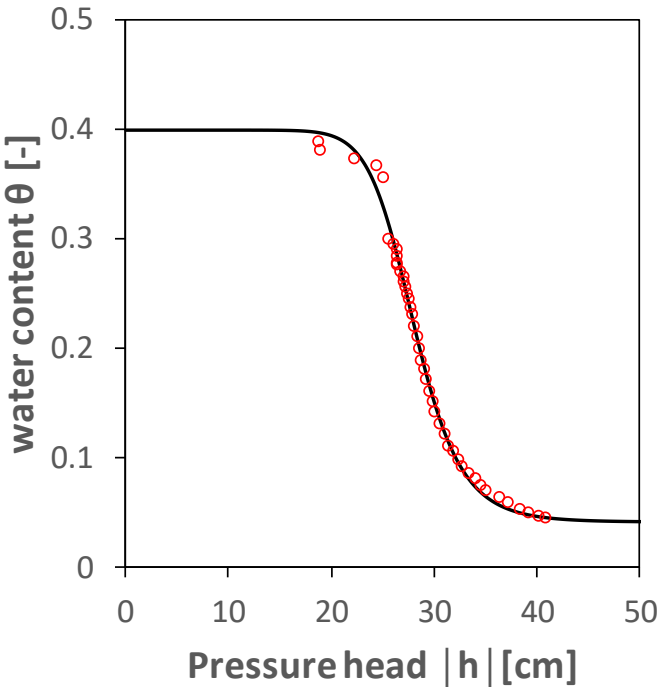

Figure 2-8. Fitting result of retention curve with van Genuchten model. The red circles represent observed data and the solid line is the simulated retention curve.

2.5.2. List of information for hydraulic model

The hydraulic model was finalized with all information acquired. ***Table 2-1*** listed all the hydraulic information and parameter required to complete the hydraulic model. They may be subdivided into three categories based on the model requirements. The first category is the hydraulic information which is to fill the Richards equation. It includes the geometry of the sand column, boundary condition of the study area, and basic hydraulic properties (porosity φ and saturated hydraulic conductivity K_s). The second category consists of retention relationship model parameters. In this case, they are the five van Genchten model parameters (θ_s, θ_r, α, *n*, and *m*). The last category is parameter(s) for unsaturated

hydraulic conductivity model. Here it is Mualem parameter *l*. All information mentioned above must be obtained prior to building variably saturated porous medium model.

Table 2-1. list of hydraulic properties and model parameters

Geometry	Boundary Conditions		Hydraulic Properties			van Genuchten Parameters				
D	q_{in}	h_{lb}	φ_c	φ_f	K_s	θ_s	θ_r	α	n	m
cm	cm/hr	cm	-	-	cm/hr	-	-	cm^{-1}	-	-
24	0.44	-20.2	0.4	0.35	194	0.4	0.04	0.04	12.7	0.9

D = Ottawa sand column depth

q_{in} = inflow velocity (upper boundary condition)

h_{lb} = capilllary pressure head at sand column bottom (lower boundary condition)

φ_c = porosity of coarse Ottawa sand

φ_f = porosity of fine Berkeley Springs sand

K_s = saturated hydraulic conductivity

θ_s = saturated water content (it is assumed equal to porosity)

θ_r = residual water content

α = van Genuchten model parameter

n = van Genuchten model parameter

m = van Genuchten model parameter; it is assumed a fixed relationship between m and n: m = 1 - 1/n

2.5.3. Water Content Distribution

Model simulation result was shown in ***Figure 2-9***. The curve on the righet side is the simulated water content distribution along the sand column depth. As seen in the figure, the water content increased from 0.08 to 0.40 over the depth. This indicates a variably saturated condition in the sand column. The distribution of water content is S-shape curvilinear. It increased very slowly above depth -10 cm and below -20 cm, over 80% water content was increased in the -10 cm ~ - 20 cm zone. The water content at the bottom was very close to 0.40, which indicated that the bottom was nearly saturated. The black dots are observed water content values at 7 cm and 17 cm above model bottom.

The simulated curve is very close to them. Flow rate at each node is constantly 0.44 cm/hour. It is symbol of steady and uniform state flow in the sand column.

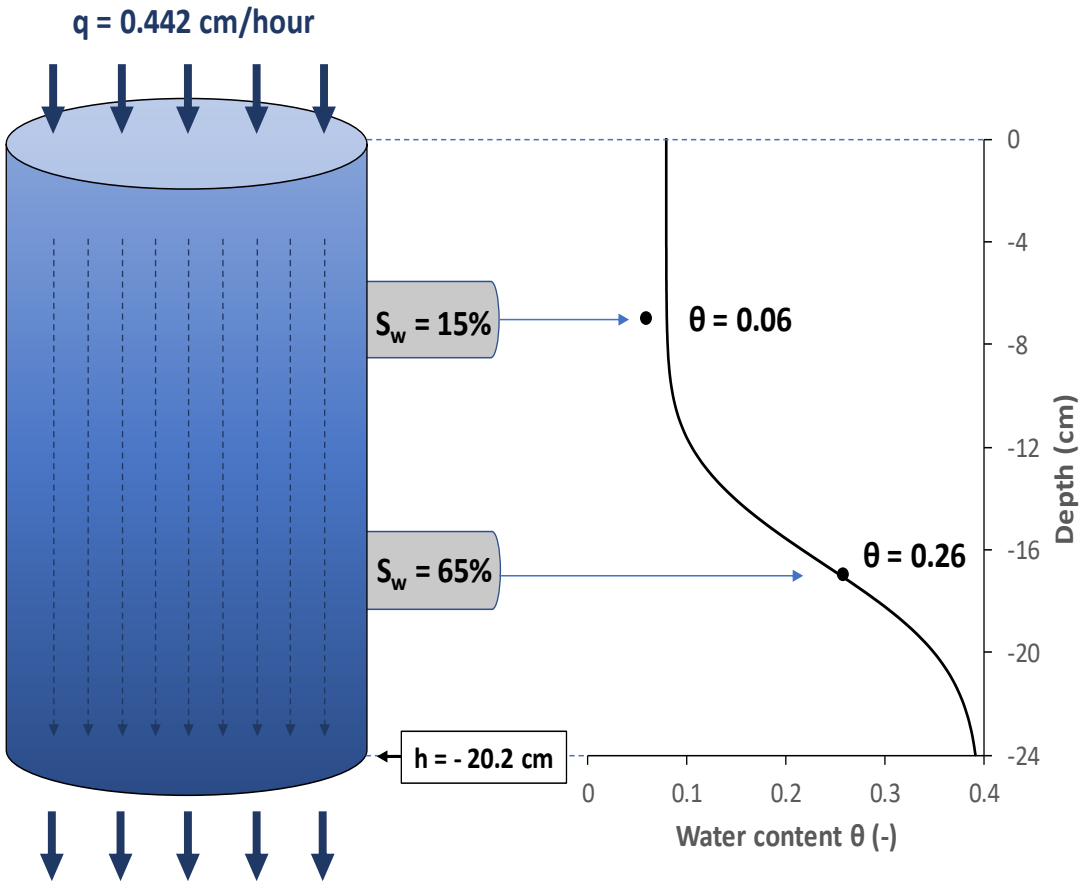

Figure 2-9. Hydraulic model for transport experiment and water content distribution. The blue column on the left side is the conceptual model of the sand column. It shows boundary conditions at both ends and the observed moisture at 7 cm and 17 cm above the model bottom. The solid line on the right side is the water content distribution along the depth.

3. Surfactant-Enhanced Bacteria Transport

3.1.Summary

It was reported that bacteria transport in porous media was enhanced by presence of surfactant. Several types and concentrations of surfactant were investigated in this study. Laboratory result shows that surfactant effect on bacteria (*E. coli*) causes two main changes: 1) decreasing cell breakthrough time; 2) increasing cell effluent concentration. The enhancement effect increases with the surfactant concentration. And anionic surfactant has significantly stronger effect than nonionic surfactant. Bromide tracer transport tests in presence of different type and concentration of surfactant showed very similar breakthrough pattern, which indicated surfactants had no impact on hydraulic condition in the sand column.

Mathematical model accounts for this phenomenon was developed in this study basing on laboratory data. Advection-dispersion equation coupled with one kinetic sorption site and size exclusion coefficient was found fit the observe data well. Dispersion coefficient was obtained by inversing bromide tracer breakthrough data. Peclet number is much larger than 6 which implied an advection dominated flow in the sand column. The goodness of fit r^2 for all cell breakthrough data matching tests are above 0.9, which indicates excellent model compatibility for different types and concentrations of surfactant. The model has two controlling parameters: deposition coefficient (k) and size exclusion coefficient (θ_{im}). Sensitivity test on controlling parameters showed that increasing k only decreased cell effluent concentration (C/C_0), while increasing θ_{im} increased cell effluent concentration (C/C_0) and also shortened cell breakthrough time (t_b).

3.2. Introduction

Bacteria are microorganisms prevailed in subsurface. They display a great diversity in shape and they are typically 0.5 ~ 5 μm in length [63], [64]. Surfactants are chemical organisms widely used in domestic detergents. When existing in aqueous phase, they tend to absorb onto interfaces thus change the surface tension of the interface. Both bacteria and surfactants are rich in domestic waste water. Recent research found that surfactant enhance bacteria or other colloids transport in porous media [8], [14], [15], [28]. PI's laboratory study indicated that the addition of surfactants significantly impacted the transport of bacteria through the sand column. Two main changes in the breakthrough curves are 1) the decrease in breakthrough time (t_b) and, 2) the increase of the effluent relative effluent cell concentration (C/C_0). However, to the best of the author's knowledge, mechanisms behind the phenomenon has not been thoroughly studied. An understanding of bacteria transport in presence of surfactants in subsurface is of immense importance for many practical scenarios.

Considerable research has been devoted to the fate and transport of bacteria or other colloids in unsaturated porous media [65]–[67]. Traditional bacteria transport models are generally described by the advection-dispersion equation with modification to account for deposition, growth, and decay of bacteria [68]–[70]. Colloidal advection is defined as mass flow of colloids due to water flux. The direction and rate advection is related to the water flux. Dispersion equations are the combination of several processes, due to the complexity of porous media structures and the diversity of water fluxes within the media [39], [46]. Dispersion is usually depicted using Fick's law.

The main challenge of developing surfactant-enhance bacteria transport model is to account for effect of surfactants with reasonable modifications on advection-dispersion model. Deposition is a widely recognized mechanism of bacteria travelling in porous media. Deposition can be caused by gravity, DLVO (Derjaguin-Landau-Verwey-Overbeek theory) forces, and non-DLVO forces [71]. DLVO is the traditional theory for colloid-surface interactions, where the total interaction energy between colloids and interfaces (Φ_{total}), e.g., solid-water interface (SWI) and air-water interface (AWI), is calculated as the sum of the repulsive electrical double layer energy (Φ_{dl}) and the attractive van der Waals interaction energy (Φ_{vdW}) [71], [72]. There is a growing body of literature suggesting that colloid behavior, in some cases, is not consistent with DLVO due to non-DLVO interactions, e.g., hydrophobic interaction, capillary forces. Extended to the pore scale, colloids can also be trapped by narrow pore spaces through physical straining, e.g., grain-grain contacts, thin water film [19], [72]. Size exclusion is another common phenomenon in porous media. Studies found that the large size colloid breakthrough earlier than solute tracer [73]–[75]. The explanation is that colloids are excluded from small size pores when they are travelling in the porous media. Colloid are physically constrained in the relatively larger pores which is more conductive than small pores. Hence, the bacteria average transport rate is increased.

The objective of this Chapter is to develop a numerical model which can account for surfactant-enhanced bacteria transport. It was achieved by modifying advection-dispersion equation with possible processes of bacteria transport in porous media and validating with observed data. Section 3.3 briefly introduced the *E. coli* transport experiment and its result. Section 3.4 specifically explained how the model was

developed including selecting governing equations, adjusting observed data, and inversing dispersion coefficient. Section 3.5 displayed the model simulating results under different types and concentrations of surfactants. Sensitivity analysis on controlling parameters of the model was also shown in this section.

3.3. Laboratory Experiment

Bacteria transport experiment was conducted by Tripathi and Brown. Nonionic surfactants (Brij 30 and Brij 35) and anionic surfactant (linear alkylbenzene sulfonate) were investigated for their impact on *E. coli* transport through an unsaturated sand column.

3.3.1. Materials

3.3.1.1. Sand Column

The sand column was described in Chapter 2. It was packed with 24 cm coarse Ottawa sand. A thin layer of fine Berkeley Springs sand was placed at the bottom to prevent the formation of capillary fringe. The sand column was kept unsaturated with a constant water content distribution along the depth. The water flow in the column was remained steady at the same flow rate for all transport experiment.

3.3.1.2. *E. coli* Preparation

1. *Escherichia coli* K-12 (ATCC 29181) were grown for 2 days in 500 mL minimal media until they reached the stationary growth phase of the culture.
2. Plates were washed three times with buffer solution (PBS), starved overnight and washed once more the next morning.
3. Cells were stained using 5-(and 6-)-carboxyfluorescein diacetate succinimidyl ester (CFDA/SE, Invitrogen).

Two nonionic surfactants (Brij 30 and Brij 35) and one anionic surfactant (linear alkylbenzene sulfonate LAS) were investigated in this study to compare impacts on

bacteria transport by different types of surfactants. The surfactant Critical Micelle Concentration (CMC) values were measured with a DuDouy tensiometer.

Influence of surfactant mixture were also studied. LAS and one of the Brij surfactants were mixed at a specific concentration.

3.3.2. Transport experiment

Bacteria were transported across an unsaturated sand column. $CaCl_2$ solution with an ionic strength of 1 mM and pH 7 was used as the baseline of the transport experiment. Various concentration surfactants were added to the baseline solution depending on the type of surfactant. For nonionic surfactant Brij 30 and Brij 35, the surfactant solution concentration was controlled at 0.5, 1, 2, and 6 times the CMC of the two surfactants; For anionic surfactant LAS, it was at 0.25, 0.5, 0.75, 1, and 2 times CMC of LAS.

1. Conditioning: baseline solution passed through the sand column for 12 hours prior to each run at a flow rate of 0.442 cm/hour.
2. Tracer test: bromide solution (mM NaBr) confirmed the consistency of the hydraulic conditions for each test
3. Test start: test solutions were pumped at 0.7 mL/min through the sand column.
4. Sampling: effluent was collected using a fraction collector
5. On-line analysis: effluent bacterial concentration was determined using direct counting via epifluorescence microscopy with a digital image system
6. Test completion: after effluent bacterial concentration reached an equilibrium, the feed was switched to baseline solution

3.3.3. Results

The addition of surfactants significantly impacted the transport of *E. coli* through the sand column. Cell breakthrough curves are displayed in ***Figure 3-4***, ***Figure 3-5***, and ***Figure 3-6*** in section 3.4.3.2 along with simulated results. Two main changes in the breakthrough curves are 1) the decrease in breakthrough time (t_b) and, 2) the increase of the effluent relative effluent cell concentration (C/C_0). For pure surfactant solutions, the anionic surfactant LAS has a more significant effect than the nonionic Brij surfactants. As can be observed in ***Figure 3-1***, when concentration of Brijs was increased from 0 × CMC to 2 × CMC, t_b and C/C_0 changed from 9.5 hours to 7.5 hours and 0.165 to 0.260, respectively. At the same concentration change, LAS decreased t_b to 5.67 hours, about 2 hours early than that of Brijs, and C/C_0 was 0.546, about 0.2 higher than that of Brijs. For surfactant mixtures, the LAS portion showed a more significant role in decreasing t_b, increasing C/C_o, and enhancing bacteria transport versus Brij. In tracer tests, increases in surfactant concentration did not affect results, indicating that surfactants impact on flow patterns was not significant.

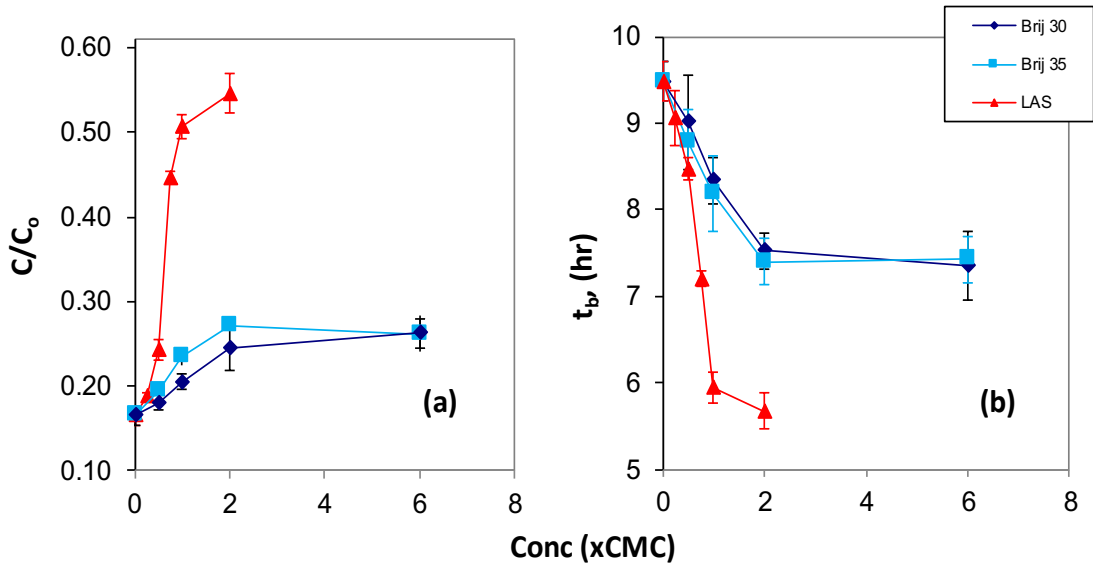

Figure 3-1. Influence of pure anionic surfactant (LAS) and pure nonionic surfactant (Brijs) on relative effluent *E. coli* cell concentration (a) and breakthrough time (b). Both types of surfactants increased relative effluent cell concentration. The higher surfactant concentration, the more significant the effect. Anionic surfactant had a stronger impact than nonionic surfactants.

3.4.Surfactant-Enhanced Bacteria Transport Model

Experimental results showed decreased *E. coli* breakthrough time and increased effluent concentration due to the presence of surfactants. A numerical model based on experimental conditions was developed to simulate laboratory results and elucidate the pertinent mechanisms.

E. coli cells are about 0.5 - 2.0 μm in diameter [76]. In this study, the movement of bacteria in porous media is assumed to be similar tno inert colloids (10 nm~10 μm) [71], [72], [77]. Much research on colloid transport in porous media has been completed and many numerical models have been developed for different purposes. However, to the best of the author's knowledge, there is no model depicting bacteria transport in unsaturated porous media under the effect of surfactant. The objective of this study was to develop such a model based on laboratory data.

3.4.1. Governing Equations

Though governing equations of colloid transport have vast variety, their fundamentals are almost the same: advection-dispersion equations with sink/source terms. This section discussed advection-dispersion equations and modifications with the mechanism models to account for the effects of surfactants.

3.4.1.1. Advection-dispersion equation

The colloid transport processes are advection, diffusion and dispersion, and reaction (sink/source) in the porous media [40]. Advection is the mass flow of colloids due to the water flux containing colloids. The direction and rate of transport of colloids is related to

the water flux. Hence, advection is calculated based on water flow pattern. Diffusion is a transport mechanism due to differences in colloid concentration between locations: colloid mass flux is proportional to the concentration gradient, i.e., Fick's first law [78], [79]. Diffusion causes the colloid front to spread and become less sharply defined. Dispersion has a similar - and greater- effect as diffusion, but through a different mechanism. Dispersion equations are the combination of several processes, due to the complexity of porous media structures and the diversity of water fluxes within the media [39], [55]. Diffusion and dispersion are usually combined as one due to their similar effect and governing equation if they are not studied separately. Form this point of the thesis on, the term of dispersion refers to the combination effect of diffusion and dispersion.

The sink/source term varies greatly, as its form depends on the study purpose or the specific transport conditions. For example, the sink/source term can be interpreted as attachment-detachment, straining, root uptake, evaporation, bacteria growth or decay. Multiple sink/source terms can be used to represent different reactions happening simultaneously. The 1-D advection-dispersion equation with reaction term is often described as a colloid mass balance equation,

Equation ***3-1***.

$$\frac{\partial \theta c}{\partial t} = \frac{\partial}{\partial x}\left(\theta D \frac{\partial c}{\partial x}\right) - \frac{\partial qc}{\partial x} + S \qquad \textbf{Equation 3-1}$$

where θ is water content [length^3/length^3]; c is colloid aqueous phase concentration [number of colloids/volume]; D is colloid dispersion coefficient [length^2/time] (to quantify the dispersion and diffusion effect); q is water flow rate [length/time]; S is sink/source rate [number of colloids/time]; t is time; and, x is spatial coordinate [length].

The left-hand side of the equation represents the mass of colloid change with time in the porous media. The first and second term on the right is the colloid mass change due to dispersion and advection, respectively. The last term S is colloid change due to colloidal reaction with porous media, i.e., sinks, sources.

3.4.1.2. Colloid Deposition and Irreversible Sorption Sites

To account for the surfactant enhancement on *E. coli* transport in the model, the sink/source term in Equation ***3-1*** must be converted to one that matches the experimental condition in this study.

It is widely recognized that colloids tend to be retained when they are travelling in porous media, the process is call retention or deposition. Deposition can be caused by gravity, DLVO (Derjaguin-Landau-Verwey-Overbeek theory) forces, and non-DLVO forces [71]. DLVO is the traditional theory for colloid-surface interactions, where the total interaction energy between colloids and interfaces (Φ_{total}), e.g., solid-water interface (SWI) and air-water interface (AWI), is calculated as the sum of the repulsive electrical double layer energy (Φ_{dl}) and the attractive van der Waals interaction energy (Φ_{vdW}): $\Phi_{total} = \Phi_{dl} + \Phi_{vdW}$ [71], [72]. If the net force is attractive, colloids move towards interfaces and stick on them. This process is called attachment.

One simple model account for colloid attachment in porous media is the classical colloid filtration theory (CFT) model. It is based on DLVO theory [80], [81]. The model lumps all effects on deposition into a single, first-order kinetic rate k [$time^{-1}$], assuming that the colloid deposition is irreversible [82]. Irreversibly deposited colloids are permanently retained in the sand column.

Other common reactions relating to microorganism transport are bacteria growth and decay. Without growth media, *E. coli* growth was assumed non-existent. Given a short hydraulic retention time, *E. coli* decay was assumed to be negligible.

3.4.1.3. Size exclusion

Size exclusion is another effect prevailing in colloid transport. It increases the mobility of colloids by physically constraining them into domain and pore networks which are more conductive and where higher flow rate exists in porous media [22]. The size exclusion effect is included by the introducing size exclusion coefficient, $\theta_{im,}$ into model. It represents the volumetric water content inaccessible to the mobile bacteria [length^3/length^3] due to size exclusion, θ was replaced with θ_c in Equation ***3-1***, where $\theta_c = \theta - \theta_{im}$. Figure 3-2 describes the concept of bacteria accessible water content. The gray column represents an unsaturated porous medium, only a portion of its pores are filled with water where water flux exists. The total water content in the porous medium is θ. Bacteria are transported by the water flux, they travel in the pores where water flux prevails. Because of the size exclusion effect, some of the pores or thin water film are shut down for bacteria. They are represented by the black circles. And the water content in black circles is θ_{im}, water content not accessible to bacteria. Then, bacteria travel with the rest of the water flux, or the water content accessible to bacteria $\theta_c = \theta - \theta_{im}$. It is shown as blue circles in the figure.

The average flow rate of the bacteria accessible region (q_c) is larger than that of the whole porous media (q). Because bacteria accessible region primarily consists of large pores in porous media which have better conductivities than smaller pores. q_c is

determined by equation: $q_c = q \times (K_{rc} / K_{rw})$, where Krc is water relative permeability [-] and K_{rw} is the bacteria accessible water relative permeability [-]. Water relative permeability is typically estimated from soil moisture retention data using a pore size distribution model. For example, K_{rw} is calculated from equation:

where r is pore radius in the porous media [length]; x is a dummy saturation variable of integration [-]; γ [-] is the water saturation is not accessible to bacteria which is equal to ratio of bacteria excluded water content (θ_{im}) to total water content (θ): θ_{im} / θ.

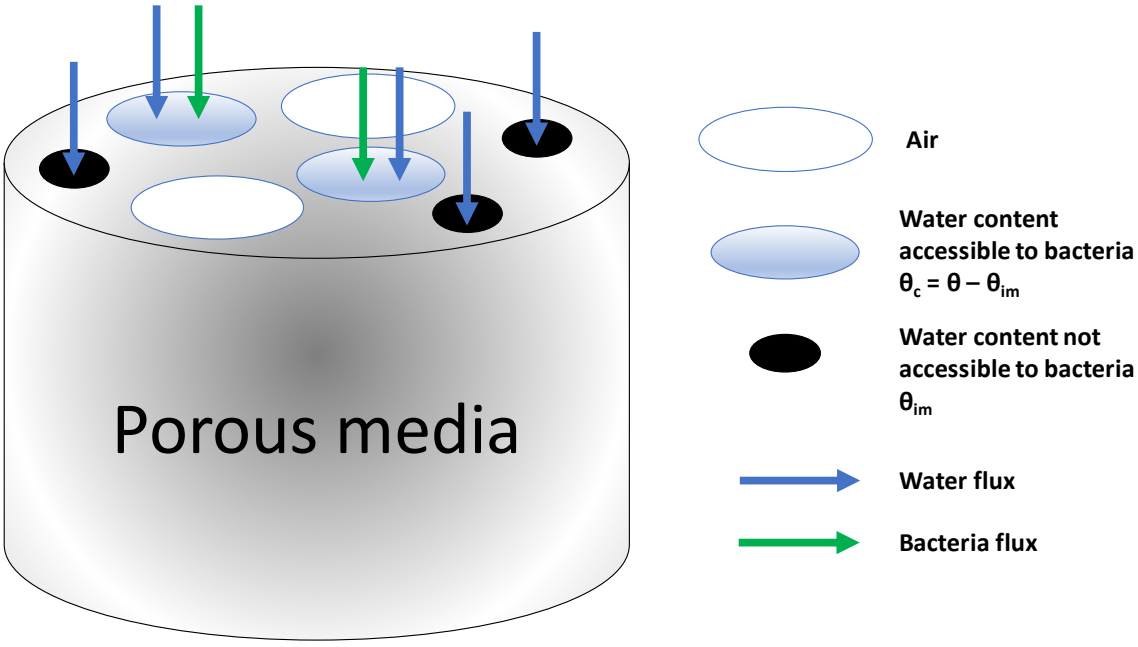

Figure 3-2. Diagram of the size exclusion effect in porous media where large colloids do not have access to all water content, e.g., bacteria. Note: blue circles are accessible water content where there is bacteria flux, black circles are inaccessible water where there is no bacteria flux.

3.4.2. Numerical Model

Advection-dispersion with one kinetic sorption site and size exclusion coefficient is the proposed surfactant-enhanced bacteria transport model in this study, expressed as Equation ***3-2***:

$$\frac{\partial \theta_c c}{\partial t} + \theta_c k c = \frac{\partial}{\partial x}\left(\theta_c D \frac{\partial c}{\partial x} \right) - \frac{\partial q_c c}{\partial x} \qquad \textbf{Equation 3-2}$$

The model is highly nonlinear and solved numerically using finite element HYDRUS 1D code. It has the same model discretization as the hydraulic model mentioned in Chapter 2 except the nodes now also stores bacteria transport information, e.g., cell concentration. In the surfactant-enhanced bacteria transport model for an unsaturated sand column, Equation ***3-2***, there are three unknown parameters: deposition rate coefficient (k), size exclusion coefficient (θ_{im}), and dispersion coefficient (D). θ_{im} and k were obtained by optimizing fit with *E. coli* breakthrough curves. D was determined by optimizing fit with bromide breakthrough curves. Hydrus-1D code was found to be a suitable solver for the extensive inverse calculations required to optimize the parameters. The code is capable of fitting model parameters with observed breakthrough data using a nonlinear least square optimization routine based on the Levenberg-Marquardt algorithm [35], [83].

According to the bromide tracer test result, surfactant impact on hydraulics was insignificant; only parameters k and θ_{im} are affected by surfactants. By assuming that surfactants don't affect hydraulic conditions in the sand column, the result of the hydraulic model from Chapter 2 was directly input into the bacteria transport model without any modification for type or concentration of surfactants. It means that hydraulic information at each node of bacteria transport model was the same that of hydraulic

model at steady state. The dispersion coefficient was determined by inversing Bromide tracer data (see section), the parameters left to be optimized are k and θ_{im}.

Prior to fitting data to the observed bromide and *E. coli* transport data, the data was preprocessed by shifting time 0.8 hour earlier to eliminate the discrepancy between experimental and model geometry.

3.4.2.1. Data adjustment

The discrepancy is that the model doesn't account for the experimental setup with 1cm fine sand on the bottom of the column because it is not possible to obtain some hydraulic properties of the mud-like fine sand with basic hydraulic and Geotech laboratory apparatus. Bradford (2002) observed that colloidal straining occurs primarily near the surface of the sand column. Deposition dramatically decreased as increasing depth [19]. Hence, it was assumed that the fine sand only extends the travel length and travel time. The observed transport data represents the particles passing through 1) 24cm coarse Ottawa sand and 2) 1cm Berkeley Springs fine sand. Significant errors would occur if the original observed data was applied directly to the model. Any changes to colloid transport by the fine sand versus coarse sand should impact all results evenly.

The actual velocity in the fine sand v_{af} can be calculated by $v_{af} = q / n_f$, where q is the Darcy velocity [length/time], which is 0.44 cm/hour; and n_f is the porosity of the fine sand which is 0.35. Then, the traveling time through 1 cm fine sand was calculated, which is about 0.8 hour. This time was subtracted in all data points by advancing them 0.8 hour.

3.4.2.2. Inversing Dispersion Coefficient

The bromide transport result in the presence of surfactants revealed that the surfactant had no noticeable influence on flow pattern or dispersion in the sand column. The *E. coli* dispersion coefficient, D, in Equation ***3-1*** was acquired separately from conservative bromide tracer tests by assuming *E. coli* cells disperse similarly as bromide tracer.

The transport of the tracer was assumed to have no reaction in the sand column [84] and to be governed solely by advection and dispersion. Hence, governing equation of bromide tracer transport is the basic advection-dispersion equation. The only unknown parameter was the dispersion coefficient (D). It was determined using parameter optimization method which is discussed in Chapter 2 by matching observed bromide breakthrough data. This approach was applied on twenty-five separate bromide tests. These tests are in presence various type and concentration of surfactants.

Peclet number (P_e) of each test was calculated to determine dominating transport effect (advection or dispersion). Peclet number (P_e) is a dimensionless number used to compare strength of advection and dispersion effect in groundwater [85]: $Pe = v \times d / D$, where v is the average linear water flow velocity [length/time], here it is estimated by $q/\theta_s = 483$ cm/hour; d is the average sand grain diameter [length] which is 0.0275 cm.

3.4.3. Results

3.4.3.1. Dispersion coefficient

Advection-dispersion equation simulation fits observed bromide tracer data fairly well. ***Figure 3-3*** presents an example of fitting result (Test number 7). Dots and solid line represents observed and simulated breakthrough data, respectively. As can be seen from

the figure, discrepancy between observed and simulated data is very small, goodness of fit coefficient r^2 is above 0.90 which indicates an excellent fit. And dispersion coefficient yielded by the model is reliable. All other twenty-four tests showed similar fitting results (data are not shown).

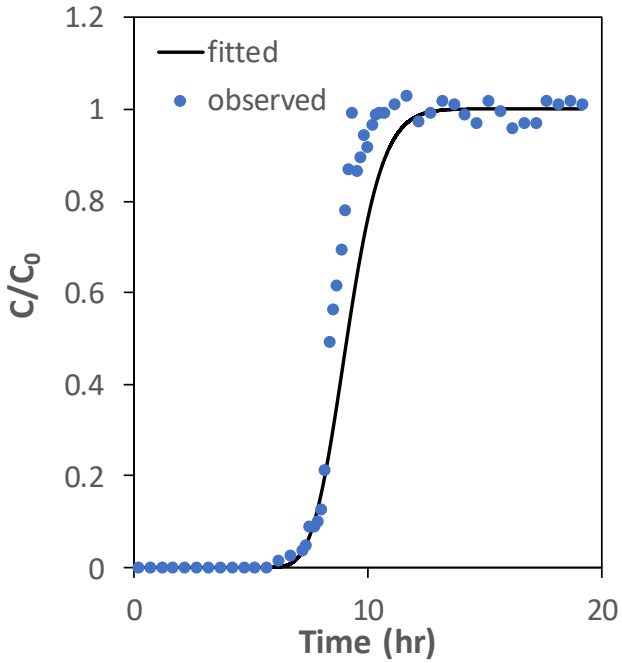

Figure 3-3. Fitting result of advection-dispersion equation with observed bromide breakthrough data.

Table 3-1 displays dispersion coefficient (D) values over twenty-five tests ranged from 0.06 to 0.30 cm2/hour. And all Pe number are much greater than 6 which indicates overwhelmingly advection-dominated flow in this study. As the effect of dispersion weighed insignificantly effects on flow pattern, it was not necessary to measure dispersion coefficient with high accuracy. An average D value (0.16 cm2/hour) was used and kept constant in bacteria transport model.

Table 3-1. Dispersion coefficients and Peclet numbers over twenty-five tests. Note: P_e > 6 indicates advection-dominated flow.

Test Number	Dispersion Coefficient (cm^2/hour)	Peclet Number (-)
1	0.15	90.30
2	0.17	79.00
3	0.13	99.10
4	0.13	98.80
5	0.10	130.94
6	0.21	64.14
7	0.09	145.53
8	0.06	221.51
9	0.11	125.50
10	0.20	65.22
11	0.08	166.41
12	0.09	149.57
13	0.21	63.34
14	0.13	99.10
15	0.13	99.10
16	0.10	130.97
17	0.10	138.02
18	0.14	95.18
19	0.14	97.15
20	0.19	68.92
21	0.22	60.65
22	0.29	46.28
23	0.22	61.43
24	0.23	57.33
25	0.30	44.52

3.4.3.2. Compatibility of Surfactant-Enhanced Bacteria Transport Model

Advection-dispersion equation with one kinetic sorption site and size exclusion coefficient provided a robust fitting result with observed *E. coli* breakthrough data. The following sections examined model compatibility for different types of surfactants: anionic, nonionic, and mixtures.

For pure surfactant, ***Figure 3-4*** (a), (b), and (c) present fitting results of surfactant-enhanced bacteria transport model in presence of anionic surfactant LAS, nonionic

surfactant Brij 30 and Brij 35, respectively. Markers in each shape represent observed *E. coli* breakthrough data in presence of surfactant at a certain concentration. The corresponding surfactant concentration can be found at the right side of the breakthrough curve. Solid lines close to each type of markers are model simulated E. coli breakthrough for each observed breakthrough data. Simulating results fit well with the observed data.

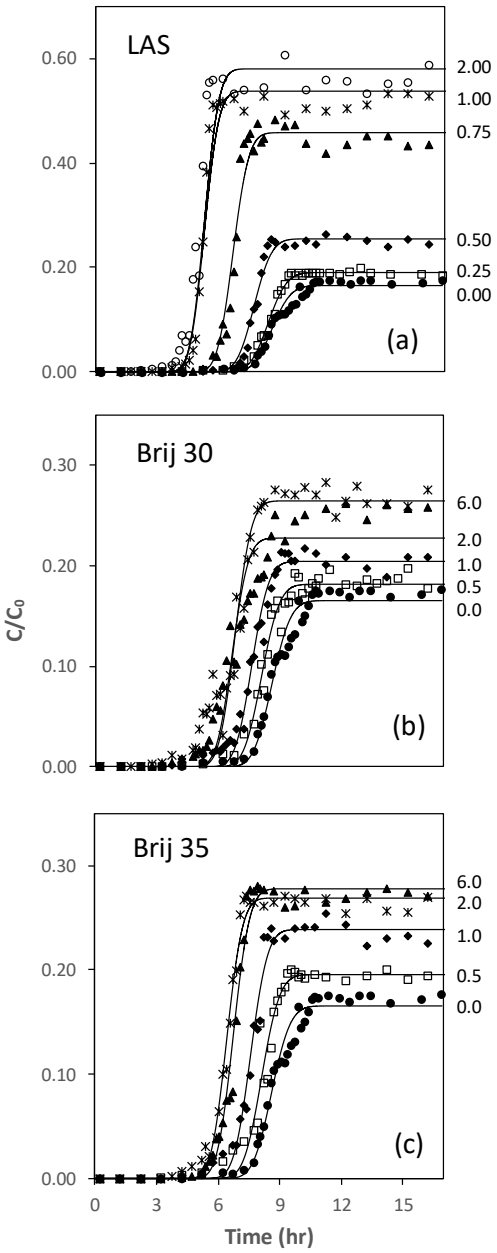

Figure 3-4. Fitting result of observed and model simulated *E. coli* breakthrough curves in presence of mixture of anionic surfactant LAS (a), nonionic surfactant Brij 30 (b), and Brij 35. Markers in each shape represent observed data in presence of a certain concentration of surfactant. And the solid line close to each type of markers is the corresponding model simulated breakthrough curves for each set of observed data.

Table 3-2 provides a summary of the fitted model parameters: deposition rate coefficient, k, and size exclusion coefficient θ_{im}. as well as statistical information on goodness-of-fit (95% confidence interval on fitted parameters and the linear regression coefficient r^2). All the goodness of fit coefficient r^2 are above 0.93 which indicate excellent compatibility of the model.

Table 3-2. Summary of the fitted model parameters: deposition rate coefficient (k) and size exclusion coefficient (θ_{im}). Note the 95% confidence interval and the linear regression coefficient (r^2) for each set of fitted parameters.

Conc (xCMC)	Parameter				
	k (hour^{-1})		θ_{im} (-)		r^2
	value	95% C.I.	value	95% C.I.	
		LAS			
0	2.0E-01	± 3.8E-03	1.4E-02	± 1.3E-03	0.978
0.25	2.0E-01	± 2.8E-03	1.9E-02	± 9.7E-04	0.993
0.5	1.8E-01	± 5.8E-03	3.2E-02	± 1.6E-03	0.983
0.75	1.2E-01	± 6.1E-03	4.5E-02	± 1.6E-03	0.978
1	1.2E-01	± 7.3E-03	7.8E-02	± 2.6E-04	0.974
2	1.0E-01	± 1.3E-02	7.8E-02	± 4.4E-04	0.936
		Brij 30			
0	2.0E-01	± 3.8E-03	1.4E-02	± 1.3E-03	0.978
0.5	2.1E-01	± 4.7E-03	2.5E-02	± 1.6E-03	0.981
1	2.1E-01	± 5.5E-03	2.7E-02	± 1.6E-03	0.984
2	2.2E-01	± 1.2E-02	5.2E-02	± 2.8E-03	0.938
6	1.9E-01	± 9.2E-03	4.9E-02	± 2.5E-03	0.962
		Brij 35			
0	2.0E-01	± 3.8E-03	1.4E-02	± 1.3E-03	0.978
0.5	2.0E-01	± 6.9E-03	2.5E-02	± 2.2E-03	0.969
1	1.9E-01	± 5.6E-03	2.8E-02	± 1.5E-03	0.983
2	1.9E-01	± 5.4E-03	5.1E-02	± 1.3E-03	0.985
6	2.0E-01	± 9.7E-04	5.7E-02	± 4.2E-03	0.977

For surfactant mixtures, ***Figure 3-5*** and ***Figure 3-6*** display fitting results of Brij 30 + LAS mixtures and Brij 35 + LAS mixtures respectively. In each of small figure, concentration of Brij 30 or Brij 35 is fixed and can be found at upper-left corner. Markers

in each shape represent observed *E. coli* breakthrough data in presence of Brij 30 or Brij 35 mixing with LAS at a certain concentration. The LAS concentration can be found at the right side of the breakthrough curves. Solid lines close to each type of markers are model simulated E. coli breakthrough for each observed breakthrough data. Simulating results for mixture also fit well with the observed data.

Table 3-3 and ***Table 3-4*** provide a summary of the fitted model parameters: deposition rate coefficient, k, and size exclusion coefficient θ_{im} for mixtures Brij 30 + LAS and Brij 35 + LAS, respectively.

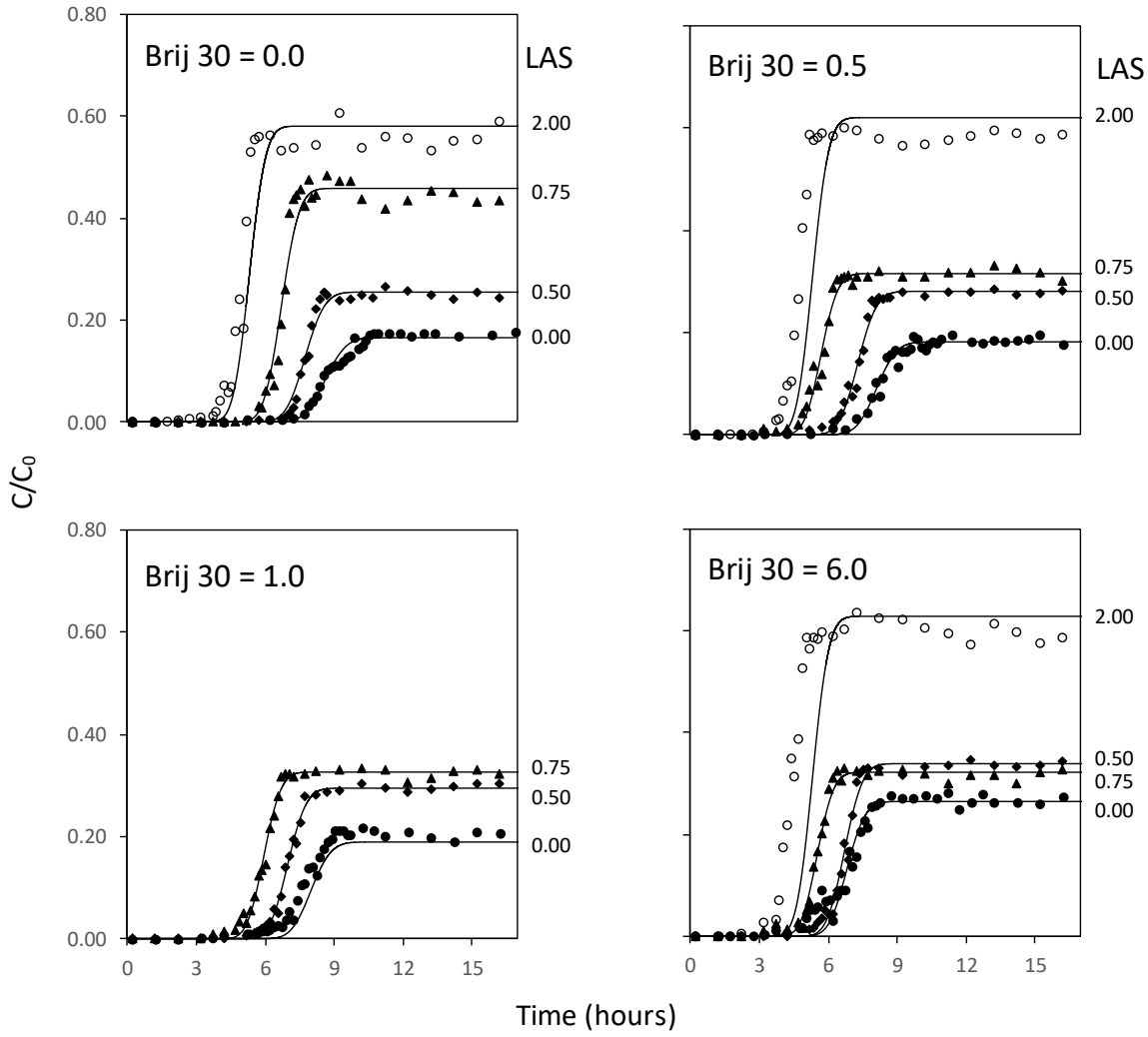

Figure 3-5 Fitting result of observed and model simulated *E. coli* breakthrough curves in presence of mixture of anionic surfactant LAS and nonionic surfactants Brij 30. Markers in each shape represent observed data in presence of a certain concentration of LAS in the mixture. And the solid line close to each type of markers is the corresponding model simulated breakthrough curves for each set of observed data.

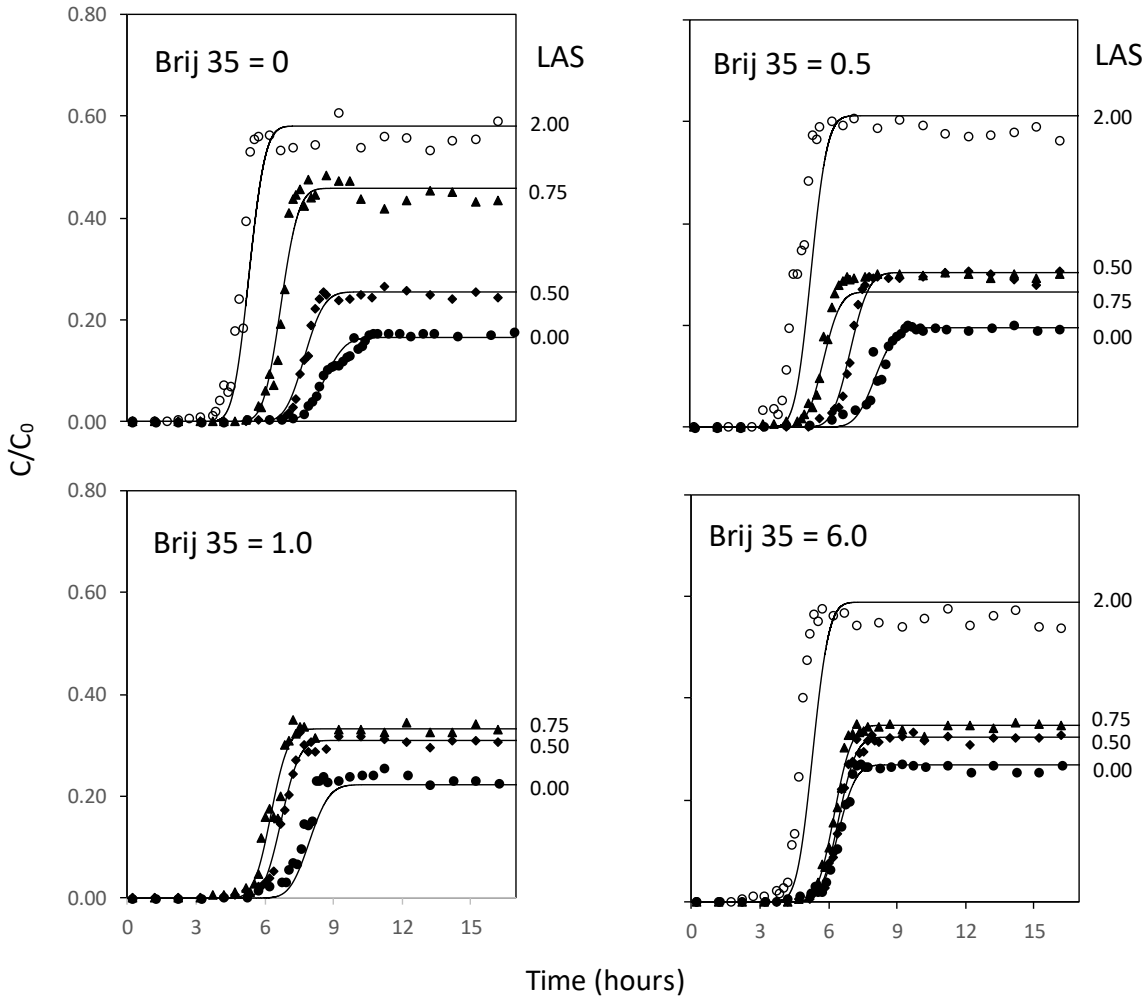

Figure 3-6 Fitting result of observed and model simulated *E. coli* breakthrough curves in presence of mixture of anionic surfactant LAS and nonionic surfactants Brij 35. Markers in each shape represent observed data in presence of a certain concentration of LAS in the mixture. And the solid line close to each type of markers is the corresponding model simulated breakthrough curves for each set of observed data.

Table 3-3. Summary of the fitted model parameters for mixture of LAS and Brij 30: deposition rate coefficient (k) and size exclusion coefficient (θ_{im}).

θ_{im} (-)		**Brij 30 conc (xCMC)**			
		0	0.5	1	6
LAS conc (xCMC)	0	1.4E-02	2.5E-02	2.7E-02	4.9E-02
	0.5	3.2E-02	4.1E-02	4.6E-02	5.2E-02
	0.75	4.5E-02	7.0E-02	6.6E-02	7.4E-02
	2	7.8E-02	7.8E-02	-	7.8E-02
k (hour^{-1})		**Brij 30 conc (xCMC)**			
		0	0.5	1	6
LAS conc (xCMC)	0	2.0E-01	2.1E-01	2.1E-01	1.9E-01
	0.5	1.8E-01	1.7E-01	1.7E-01	1.6E-01
	0.75	1.2E-01	2.0E-01	1.9E-01	2.0E-01
	2	1.0E-01	9.0E-02	-	8.7E-02

Table 3-4. Summary of the fitted model parameters for mixture of LAS and Brij 35: deposition rate coefficient (k) and size exclusion coefficient (θ_{im}).

θ_{im} (-)		**Brij 35 conc (xCMC)**			
		0	0.5	1	6
LAS conc (xCMC)	0	1.4E-02	2.5E-02	2.8E-02	5.7E-02
	0.5	3.2E-02	4.5E-02	5.1E-02	5.7E-02
	0.75	4.5E-02	6.7E-02	6.0E-02	6.0E-02
	2	7.8E-02	7.8E-02	-	7.8E-02
k (hour^{-1})		**Brij 35 conc (xCMC)**			
		0	0.5	1	6
LAS conc (xCMC)	0	2.0E-01	2.0E-01	1.9E-01	2.0E-01
	0.5	1.8E-01	1.7E-01	1.7E-01	1.7E-01
	0.75	1.2E-01	2.2E-01	1.7E-01	1.7E-01
	2	1.0E-01	9.2E-02	-	1.0E-01

3.4.3.3. Sensitivity test

The simulation results were only controlled by the deposition rate coefficient (k) and size exclusion coefficient (θ_{im}) in this model. A sensitivity analysis was performed on these two controlling parameters. Figure 3-7 shows the trend of breakthrough curves as the

values of k or θ_{im} change, where the soil hydraulic and solute transport parameters were otherwise kept constant. When θ_{im} was increased from 0.000 to 0.078, the breakthrough time was shortened and the effluent breakthrough concentration increased. As the k value decreased, the effluent breakthrough concentration increased; no obvious change was observed on breakthrough time. By comparing the two shaded areas, the functions of the two controlling parameters in bacteria transport model could be observed: θ_{im} is the only parameter that decreased breakthrough time; both θ_{im} and k contributed to increasing cell breakthrough.

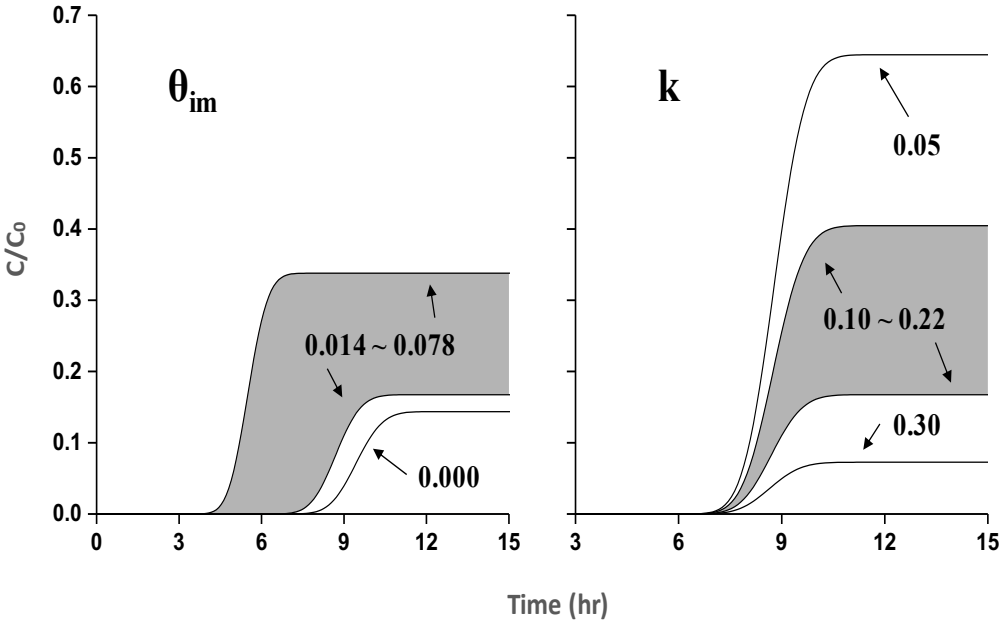

Figure 3-7. (Left**)** Time of breakthrough and C/C_o breakthrough concentration increased as θ_{im} is increased. (Right) Effluent C/C_o breakthrough concentration decreased as k increased. Note: Left: the shaded are represents C/C_o when θ_{im} is between 0.014-0.078; Right: the shaded area represents C/C_o when k values range between 0.10-0.22.

4. Surfactant-Enhanced Size Exclusion Effect

4.1.Summary

It was reported that size exclusion effect enhances colloid mobility by constraining colloids in relatively large pore space which is more conductive. This study presents numerical evidence of size exclusion by comparing fitting results from model including and model lacking size exclusion coefficient (θ_{im}). Size exclusion coefficient (θ_{im}) greatly improved model fitting result which indicated the significance of size exclusion effect. Values of size exclusion coefficient (θ_{im}) increased with increasing surfactant concentration. And values in presence of anionic surfactant LAS are obviously larger than that of nonionic surfactants Brijs at the same concentrations. This is might due to the negatively charged anionic surfactant LAS enhanced the electrostatic repulsion between *E. coli* and interfaces in the porous media. The critical pore radius of size exclusion shows similar trend as size exclusion coefficient: the higher concentration, the larger critical pore radius; critical pore radius in presence of anionic is larger than that of nonionic surfactants. The relative size of pore throats and colloids (T/C ratio) in presence of surfactant was found to be 40 – 160, which is over 30 times without the influence of surfactants.

4.2. Introduction

It was reported that, in saturated porous media, colloids migrated significantly faster and longer distance than predicted by typical approach [74], [86], [87]. Considerable column experiments showed that bacteria or other colloidal particles breakthrough earlier than conservative tracer [87]–[89]. Explanations have been proposed for this phenomenon. For example, some researchers hypothesized that large size colloids diffuse too slowly relative to solute to enter the low water velocity regions [87]; others suggested that colloids can only travel in the pores several times larger than their size and move along the faster streamlines in the pores [90]. Most of the explanations share the idea that mobility of colloids is increased by limiting in the relatively larger pores which are more conductive. This effect is referred as size exclusion effect.

Sirivithayapakorn and Keller (2003) provided evidence regarding the effect of size exclusion by observing colloids excluded from areas of small aperture size in a pore scale physical micromodel. They hypothesized the occurrence of size exclusion is dependent on ratio of pore throat to colloid diameter (T/C ratio). The ratio was reported to be about 1.5 rather than 1.0 according to their observations since the colloids preferentially enter pores with larger throat where most of streamline is directed. And measured velocities of colloids travelling in large pores were 4-5.5 times greater than averaged pore water velocity.

Despite T/C ratio, size exclusion also occurs if the electrostatic forces between colloids and porous media interfaces are repulsive. It has been observed that dissolved anions travel faster than accompanying water molecules. Because the repulsive forces pushed

them into pore center where water velocity is faster [20], [91]. In analogy to this mechanism, negatively charged colloid may also excluded from locations adjacent to negatively charged interfaces.

Surfactants are chemical organism which is rich in domestic waste water. They are able to alter interfacial energies of surfaces by adsorbing onto interfaces in porous media [4]. Some of the surfactants modules are charged. Charged surfactant may also change electrostatic conditions on the interfaces they attaching on. Theoretically, size exclusion is noticeably influenced by surfactant. However, to the best of author's knowledge, few studies investigate surfactants impact on size exclusion effect.

The objective of this chapter is to elucidate influence of surfactants on size exclusion effect basing on the experimental and numerical results of bacteria transport in presence of surfactants. Section 4.1 provided evidence of size exclusion effect in a numerical way. Section 4.2 explored surfactant type and concentration factors impact on size exclusion by correlating size exclusion coefficient with these factors. Section 4.3 hypothesis demonstrated how surfactants affect bacteria transport in a microscale. Section 4.4 investigated critical pore size of size exclusion by reflecting bacteria excluded water content onto pore size distribution figure.

4.3.Significance of size exclusion

Colloid deposition is a prevail phenomenon in porous media. It always happens because the DLVO forces always exist. However, the occurrence of size exclusion has its threshold.

The introducing of size exclusion coefficient has a great contribution to the model goodness of fit. Solid lines in ***Figure 4-1*** presents cell breakthrough fitting results in presence of surfactant LAS from two different models. The left one is the output of classical colloid filtration theory (CFT) model. This model consists of advection-dispersion equation and one first-order kinetic sorption site. can be seen in the figure, the simulated cell breakthrough curves for almost all surfactant concentrations show temporal delay to the observed data (dots in the figure). These time lags enlarge as surfactant concentration increases, from 0.5 hour (no surfactant) to 5.0 hours (surfactant concentration is 2 × CMC). At the same time, the goodness of fit r^2 dropped dramatically from 0.890 to 0.295. This indicates that classical CFT model is applicable for normal colloid transport problems. But not for problems involving surfactant effect. The stronger the surfactant effect, the weaker the model reliability. The right one is the simulating result from the model developed in this study. It is modified from classical CFT model by adding size exclusion coefficient. The fitting result is significantly increased with this model. All the temporal delays are eliminated. And the r2 remains above 0.93 (0.936 ~ 0.993) for all surfactant concentrations. This indicates that the modified model can interpret bacteria transport in presence of surfactant LAS well. The same thing was also found on nonionic surfactant Brijs and surfactant mixtures (data are not shown). It might

be considered as a proof that surfactants enhanced size exclusion effect in this study, which had significant impact on bacteria transport.

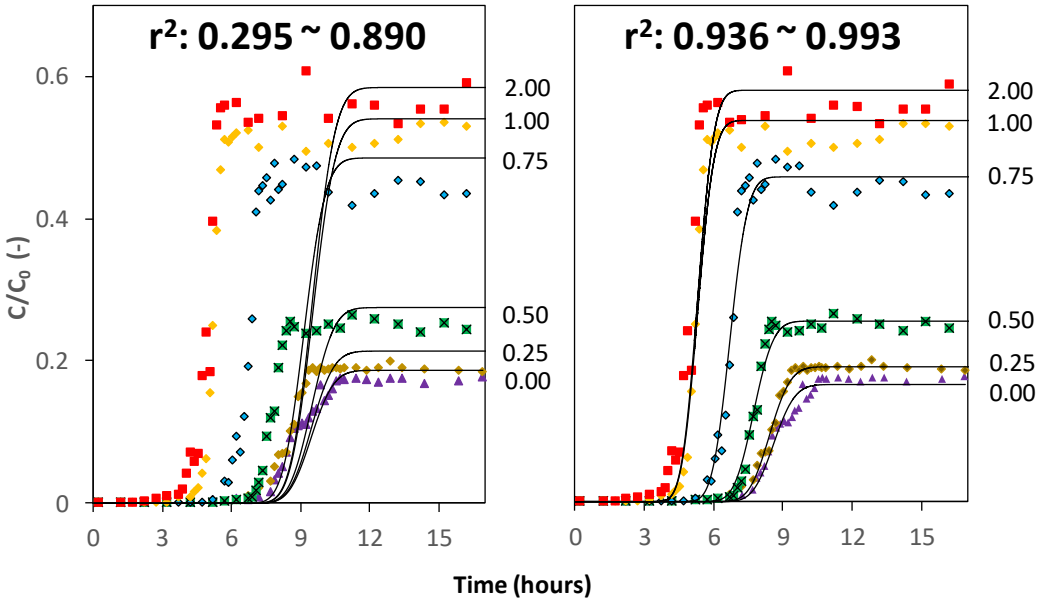

Figure 4-1. comparison of fitting results between model doesn't includes size exclusion coefficient (left) and model does (right)

4.4. Hypothesis Demonstrating of Surfactant Impact on Size Exclusion

The model result indicates that the deposition and size exclusion might be the two main processes influenced by surfactant. Figure 4-2 hypothetically demonstrates how surfactants enhance bacteria transport in pore scale. The blue background is fluid. It represents water and surfactants solution in (A) and (B), respectively. The black bars are solid phase and white bars are air phase. Interfaces between fluid and them are soil-water interface (SWI) and the air-water interface (AWI). As can be seen in the figure, pores are displayed in different sizes. Radius of center pore is larger than that of right one. The left fluid channel represents water film, it is also thinner than pore at center. At the bottom of each fluid channel is the fluid velocity profile. Generally speaking, at the same condition, the larger the pore, the closer to the center of the pore, the greater the fluid velocity. Bacteria (green bars) travels with water flow in pores and interact with SWIs and AWIs, the attractive forces (van der Waal and some non-DLVO interactions) between bacteria and the interfaces in their close proximity drives bacteria move towards and attach on these interfaces. While the repulsion between them also exist mainly due to double layer interaction and electrostatic force (bacteria and interfaces in porous media typically carry net negative charge). A microscale schematic of electrical double layer at contact with a negatively charged solid is shown at the right part of the figure. The electrical double layer refers to two parallel layers of charge surrounding the solid surface. The first layer is composed of anions attached onto solid surface due to chemical interactions. The second layer consists of cations attracted by the negative surface charge [92]. Overall, except being trapped by interfaces, bacteria are relatively unrestricted in most pores.

When surfactants (the red balls with long black tails in ***Figure 4-2*** B) in presence, they tend to sorb onto the interfaces including bacteria-water interface (BWI) in porous media. It leads to expanded electric double layer due to volume exclusion and stronger negative surface charge (if surfactants are anionic). The resulting increased repulsion pushes bacteria away from interfaces. First, bacteria are pushed in to center of the fluid channel where is high velocity region; second, if the repulsive force is strong enough, bacteria are excluded from smaller pores and thin water films into larger pores which is more conductive and with high water velocity. [71], [72], [93].Hence, because of surfactants, bacteria are less likely to attach onto interfaces or trapped at contact points between interfaces, and bacteria are transported with high velocity water flow.

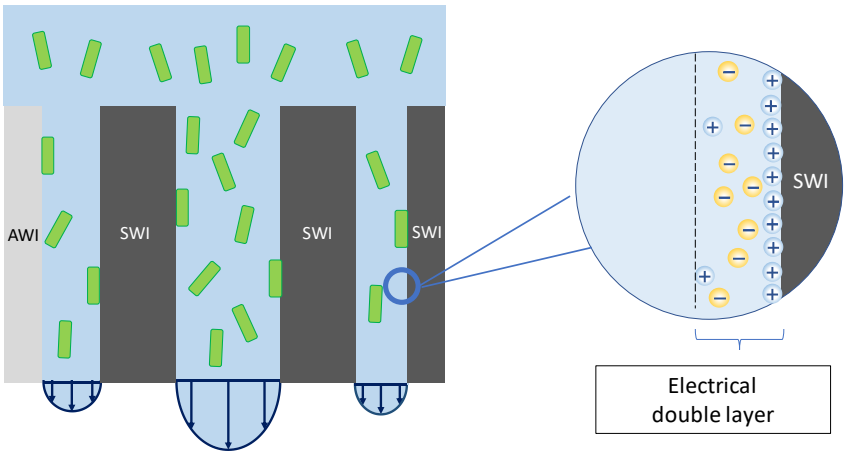

(A)

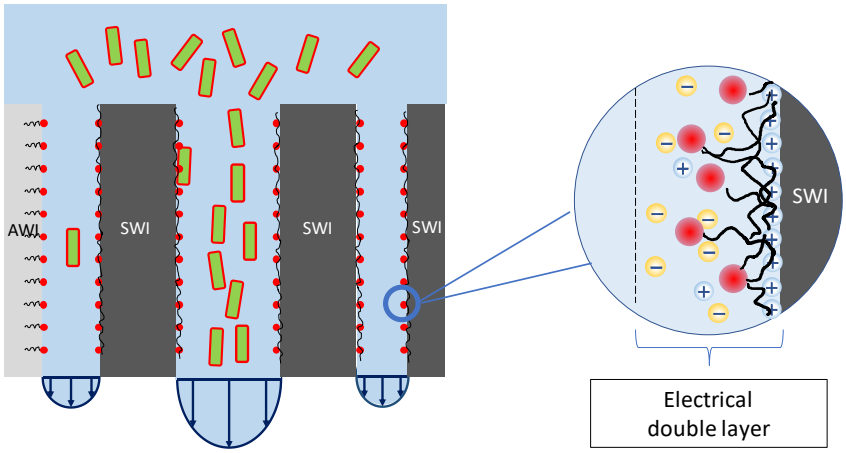

(B)

Figure 4-2 Hypothesis demonstrating of the size exclusion effect in the presence of surfactant in unsaturated porous media. (A) when no surfactant exist, bactera flow freely with bulk water. (B) surfactant sorbs at AWIs, SWIs, and BWIs. This results in expanded electric double layer due to volume exclusion effect and steric repulsion. For anionic surfactants, negative surface charge also increases, which results in a higher electrostatic repulsion. The overall result enhance the repulsion between bacteria and interfaces which pushes them to higher velocity flow regions and excluded them from smaller pores and thin water films.

4.5.Surfactant Concentration Impact

To achieve a better understanding of the surfactant concentration effect on bacteria deposition and size exclusion in porous media, relationships between concentration of three surfactants and the two controlling coefficients have been investigated. Values of k and θ_{im} for each surfactant at different concentration are shown in **Figure 4-3** (a) and (b), respectively. For the size exclusion coefficient (θ_{im}), both anionic and nonionic surfactants revealed an ascending trending with increasing surfactants concentration, showing positive quasi-Langmuir relationship. This can be well explained: Size exclusion effect was described by size exclusion coefficient (θ_{im}) in the model. Larger the θ_{im} represents stronger size exclusion effect, Hence, the positive relationship between θ_{im} value and surfactant concentration is in principle consistent with the fact that increasing surfactant concentration leads to stronger size exclusion effect. The θ_{im} values of nonionic surfactants, Brij 30 and Brij 35, are similar at each concentration and lower than those of anionic surfactant LAS. The effluent θ_{im} values of Brij 30 and Brij 35 are approximately 35% smaller than that of LAS. Tripathi and Brown (2008) found that anionic surfactant LAS had a significantly higher sorption level onto the sand than either of the nonionic surfactant Brij 30 and Brij 35. This was most likely due to the combination of higher packing density of the smaller LAS molecules; stronger sorption occurring as the hydrophilic headgroup branches off from within the alkyl chain as compared to being attached one end of the chain; and anionic surfactant LAS's negatively charged headgroup contributed to sorption to local positively charged sites on the surfaces in porous media. Therefore, LAS was more effective in enhancing bacteria

transport than Brijs in this, which led to stronger size exclusion, or larger values of θ_{im}. However, deposition coefficient k presented different patterns for the two types of surfactants. The k under effect of anionic surfactant LAS generally revealed a descending trend with increasing LAS concentration. While those for nonionic surfactants remained relatively constant. Coefficient k depicts bacteria deposition rate in the porous media. Contrary to θ_{im}, The stronger the deposition, the larger the k value. The negative relationship between k value and LAS concentration can be explained that the deposition of E. coli was weakened due to LAS sorption onto interfaces in the porous media. Higher density of LAS resulted in larger area surfactant-occupied interfaces and stronger repulsion, which led to less likely occurrence of bacteria attachment or other deposition processes in porous media. Theoretically, similar mechanisms apply in presence of nonionic surfactants Brij 30 and Brij 30. And their deposition weakening effect should not be as strong as LAS. However, k values for both nonionic surfactants Brij 30 and Brij 35 remained almost constant. The standard deviations of k for LAS, Brij 30, and Brij 35 were 0.041, 0.008, and 0.007, respectively. The amount of k value variation for anionic surfactant is about five times that for nonionic surfactants, which might indicate that the effect induced by these two nonionic surfactants was insignificant or the model is not sensitive enough to detect weak deposition.

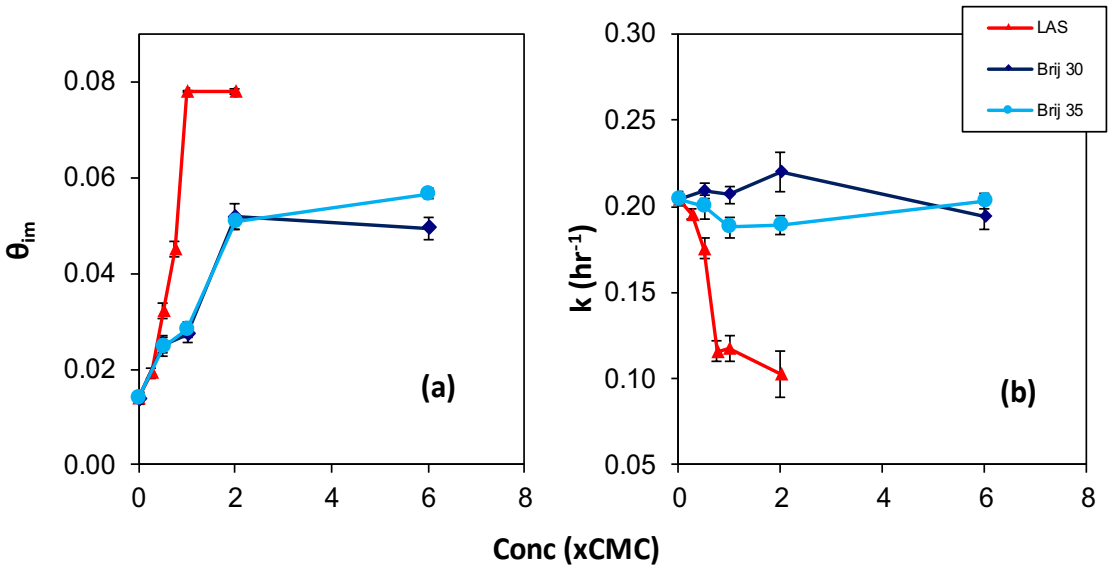

Figure 4-3 Size exclusion coefficient (θ_{im}) and deposition rate coefficient (k) change with surfactant concentration. θ_{im} increased with increase concentration for all three surfactants. k decreased with increase LAS concentration, but remain almost the same in presence of various concentration of Brij 30 and Brij 35.

One more observation worth noticing Even though there is no surfactant in the system, the surfactant concentration was 0, the θ_{im} is a small positive value rather than 0, which indicates that size exclusion effect exists though no surfactant in the system. It is confirmed by comparing the breakthrough time of E. coli and tracer. When no surfactant presents in flow, breakthrough time of bromide tracer is about 9.50 hours which is slightly longer than that of *E. coli* (about 9.48 hours). It is highly possible that size exclusion effect accelerated the *E. coli* transport. This observation is consistent with the fact that size exclusion effect may occur in natural environment.

4.6.Surfactant Impact on Critical Pore Size

This section investigated impact pure surfactants on the critical pore size for the occurrence of size exclusion. The pore structures are simplified as a bundle of capillary tubes with uniform diameters. Capillary rise function and van Genuchten retention function were used to derive pore size distribution.

4.6.1. Method

The grain particles in the sand column are not uniform in size or shape, which results the pores within them have a wide variety. Pore-size distribution is a method to quantify the relative abundance of each pore size. It is usually described by the pore size frequency function f(r) = dθ/dr, where r is the effective radius of the pores [length] [52].

Pore radius (r) may be related to capillary pressure head (h) using capillary rise law function, or Jurin's law. It suggests the height of capillary rise (h_c) is inversely proportional to the pore radius (r). And magnitude of capillary pressure head (h) is equivalent to height of capillary rise (h_c) except it is negative. Hence, capillary pressure head (h) can be expressed as a function of pore radius (r):

$$h = -\frac{2\sigma\cos(\alpha_c)}{\rho g r} \qquad \textbf{Equation 4-1}$$

Where ρ is the density of water [mass/volumn^3]; g is the gravity acceleration [length/time^2]; σ is surface tension [mass/time^2] which is approximately 7.27 × 10-2 kg/s^2 for water at 20 Celsius degree; α_c is contact angle of the water and the sand grain which is usually assumed as 0.

van Genuchten retention relationship (h *vs.* r) was used to relate pore size (r) to water content (θ). The θ(r) relationship curve is actually a cumulative pore size distribution curve. θ(r) relationship is expressed as:

$$\theta(r) = (\theta_s - \theta_r)\left\{1 + \left[2\sigma\cos(\alpha_c)\right]^n r^{-n}\right\}^{-m} + \theta_r \qquad \textbf{Equation 4-2}$$

The pore size distribution function f(r) = dθ/dr is simply the distribution of Equation 4-3:

$$\frac{d\theta(r)}{dr} = mn(\theta_s - \theta_r)\frac{\left[2\sigma\cos(\alpha_c)\right]^n}{r^{n+1} + \left[2\sigma\cos(\alpha_c)\right]^n r} \qquad \textbf{Equation 4-3}$$

Derivation of Equation 4-2 and Equation 4-3 can be found in Appendix B.

4.6.2. Result

4.6.2.1. Pore Size Distribution

Figure 4-4 (A) is the pore size frequency distribution of Ottawa sand, where x-axis is the pore radius (r), y-axis is the relative volume of pores. As observed from the figure, 0.005 cm is the dominating pore radius. Approximately 85% of pores are between 0.004 cm and 0.007 in size. ***Figure 4-4*** (B) presents cumulative pore size distribution It also describes as relationship between cumulative pore water content and effective pore radius (r). The curve shows amount of cumulative water content in the pores from the smallest to pores with a specific radius (r). And the corresponding water content value is the sum of water content in pores with a radius not greater than r. As can be seen from the curve, the cumulative water contents in the pores increases in S-shape with effective pore radius. It increases most dramatically when effective radius enlarges from 0.004 cm to 0.006 cm because pores within this radius range consist 85% of all pores. When radius beyond

0.006 cm, water content increase very mildly until reach the maximum water content which is saturated water content (θ_s).

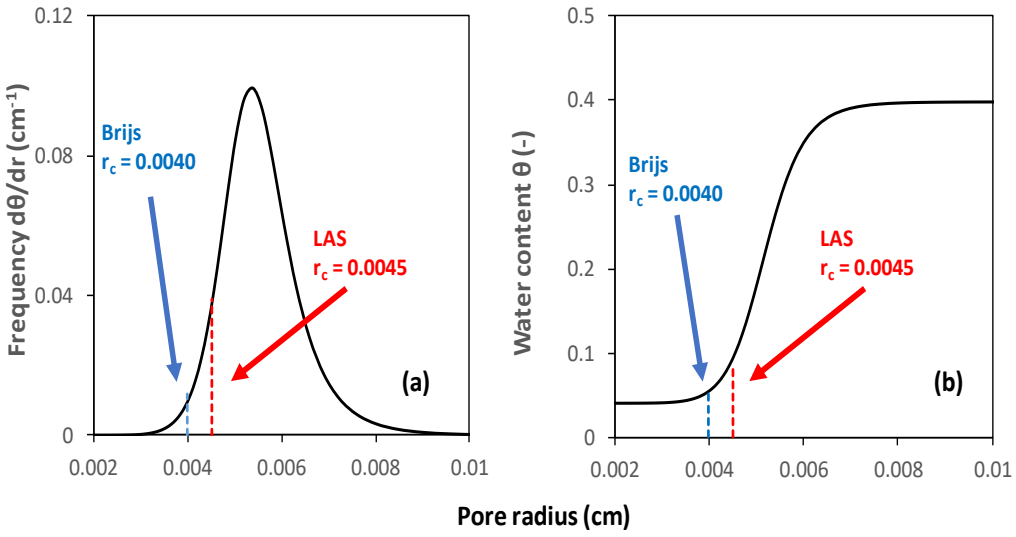

Figure 4-4 Pore size distribution (a) and cumulative pore size distribution (b). Red and blue dash lines highlight the maximum critical pore radius of size exclusion effect under the impact of anionic surfactant LAS and nonionic surfactant Brijs, respiectively.

4.6.2.2. Critical Pore Radius and T/C Ratio

Pores that bacteria excluded from can be estimated by reflecting bacteria exclused water content (θ_{im}) on to cumulative pore size distribution curve. Size exclusion shuts down pores in a small to large order, which indicates that bacteria excluded water content (θ_{im}) is water content cumulated starting from the smallest pores. As mentioned earlier, cumulative pore size distribution curve describes cumulative pore water content from the smallest to the largest pores, which is consistent with size exclusion mechanism. A corresponding pore radius(r_c) can be find for bacteria excluded water content (θ_{im}) in ***Figure 4-4*** (b). On one hand, it means the cumulative water content from pores with

radius not larger than r_c is θ_{im}; on the other hand, it indicates that pores with radius smaller than r_c are bacteria excluded. And r_c is critical pore radius.

Table 4-1 lists the critical pore radius (r_c) for pure surfactants at their different concentrations. They are calculated using the θ_{im} based on cumulative water content and pore radius relationship. For those θ_{im} smaller than 0.004, it is not possible to determine their r_c because This method is based on van Genuchten retention relationship which assumed water content cannot go down below residual water content (θ_r) which is 0.004. It can be observed from the table that, for all surfactants, as concentration of surfactant increases, critical pore radius (r_c) increases. The maximum critical pore radius (r_c) under the effect of anionic surfactant LAS is about 0.0045 cm. It is larger than that of nonionic surfactant Brijs which is around 0.0040. Maximum critical pore radius (r_t) of anionic and nonionic surfactants are marked as dash lines in ***Figure 4-4*** (b) and (b). The pores with e radius smaller than the maximum critical pore radius (r_t), or to the left of the dash lines in the figure, are the pores excluded from bacteria in the sand column due to the maximum effect of surfactants. As can be seen in (a), only a small fraction of pores was shut down under the effect of either type of surfactant, 15% for LAS and 4% for Brijs, respectively.

Table 4-1. Summary of critical pore radius and ratio of pore throat to bacteria width and length.

Conc (xCMC)	θ_{im} (-)	r_t (cm)	T/B_w ratio (-)	T/B_l ratio (-)
		LAS		
0	1.40E-02	< 0.0019	-	-
0.25	1.90E-02	< 0.0019	-	-
0.5	3.20E-02	< 0.0019	-	-
0.75	4.50E-02	0.0040	160.0	40.0
1	7.80E-02	0.0045	180.0	45.0
2	7.80E-02	0.0045	180.0	45.0
		Brij 30		
0	1.40E-02	< 0.0019	-	-
0.5	2.50E-02	< 0.0019	-	-
1	2.70E-02	< 0.0019	-	-
2	5.20E-02	0.0040	160.0	40.0
6	4.90E-02	0.0039	156.0	39.0
		Brij 35		
0	1.40E-02	< 0.0019	-	-
0.5	2.50E-02	< 0.0019	-	-
1	2.80E-02	< 0.0019	-	-
2	5.10E-02	0.0040	160.0	40.0
6	5.70E-02	0.0041	164.0	41.0

Sirivithayapakorn (2003) observed size exclusion enhanced colloid transport at a pore-scale in their lab. They hypothesis that size exclusion effect depends on the ratio of pore throat (the effective diameter of the pore) to colloid diameter (T/C ratio). When the T/C ratio is smaller than a critical value, size exclusion occurs. This threshold T/C ratio value was found to be 1.5 from their observation [17]. T/C ratio was also investigated in this study except colloid was replaced by bacteria *E. coli*, which have approximately a cubic shape about 2 μm long and 0.5 μm wide. The size change of pores and bacteria due to the sorbed surfactants was ignored. The threshold ratio value of pore throat to the *E. coli* length (T/B_l) and width (T/B_w) were calculated and listed in Table 4-1. This ratio value

increase as surfactant concentration increases. And the value of anionic LAS (45 ~ 180) is greater that of nonionic surfactant Brijs (40 ~ 160). All of them are significantly larger than the value 1.5 which was observed involving no surfactant. This result might indicate that presence of surfactant significantly enhances size exclusion. And larger pores with high T/C ratio are also excluded from bacteria.

5. Conclusions

5.1.Major contributions

This study focused on numerical method for interpreting surfactant-enhanced bacteria transport phenomenon. Its model was built to simulate and investigate the mechanisms behind the surfactant effect. The model is based on solid physical meanings and successfully matched observed bacteria breakthrough curves. The simulating result helped understand and verify the bacteria transport mechanisms affected by surfactants in variably saturated porous media. The impact of surfactant type and concentration on these mechanisms was deduced by parametric study. Surfactant impact on size exclusion threshold was studied by relating bacteria excluding water content to pore size distribution. Finally, this study provided a systematic method of studying and simulating surfactant-enhanced bacteria transport which is the basis for developing applicable model. Following sections summarized specific findings from this study.

5.1.1. Modified falling head method

The falling head method was modified in this study to achieve a more accurate K_s. The classical method used two data points to calculate K_s from Equation 2-1. Due to the small sample volume, this method is susceptible to large errors. This problem was solved by using Equation 2-1 to match a series of observed data points that present eclipsed time vs. water level in the sand column. The value of K_s in Equation 2-1was adjusted manually and corresponding r^2 was calculated. The processes were repeated until a 'best fit' was achieved. This modified falling-head method takes more data into consideration thereby reducing experimental error impact and improving the accuracy of the K value.

5.1.2. Surfactant-enhanced bacteria transport model

The main contribution of this work was developing the surfactant-enhanced bacteria transport in variable saturation porous media for the first time. The governing equation of the model is advection-dispersion equation coupled with one first-order kinetic sorption site and size exclusion coefficient. The model provides excellent on fit if observed breakthrough for all types of surfactant at all concentrations.

The model output was controlled by two parameters in the model: deposition rate coefficient (k) and size exclusion coefficient (θ_{im}). Sensitivity tests on controlling parameters shows that k only controls the effluent cell concentration C/C_0, while θ_{im} controls not only C/C_0 but also the breakthrough time.

5.1.3. Proof the significance of size exclusion

The significance of the size exclusion effect was numerically investigated. Comparison between two types of model was drawn. One of the models included size exclusion coefficient, the other one didn't. The result shows that size exclusion plays a very

important role in fitting bacteria breakthrough curves. Simulated E. coli breakthrough curves yielded from the model without size exclusion coefficient showed temporal delays comparing to observed, and the delay increased as the surfactant concentration increased. The delay was eliminated by introducing the size exclusion coefficient. This might be considered proof of the existence and significance of size exclusion effect in this study.

5.1.4. Effect of pure surfactant on controlling parameters

The correlation between controlling parameters and surfactant concentration showed different patterns for anionic LAS and nonionic surfactant Brijs. For an increasing anionic surfactant, θ_{im} increases while k decreases. Both parameters change dramatically and then mildly when LAS concentration passed 1 × CMC Threshold. This indicates that high concentration LAS has an increasing effect on enhancing size exclusion and weakening deposition. For nonionic surfactant Brijs, θ_{im} reveals a similar, weaker trend with that of LAS. However, the k remained almost constant at all concentrations. This might indicate nonionic surfactant Brijs did not have an obvious effect on preventing deposition in sand column.

5.1.5. Effect of pure surfactant on size exclusion threshold

The study provided a method to figure out the critical pore radius of the size exclusion, or radius of the largest pore excluded from bacteria. θ_{im} is the water content not accessible to bacteria due to the size exclusion effect. Under the effect of the size exclusion, pores with smaller radius are shut down for bacteria first. Hence, θ_{im} can also be considered as the sum of pore space smaller than pores with a critical radius. This radius can be obtained by relate θ_{im} to pore size distribution.

The critical pore radius increases with the increasing surfactant concentration for both type of surfactant. LAS excluded larger pores than Brijs at all concentrations which is consistent with the fact that size exclusion effect is stronger under anionic surfactant than under nonionic surfactant.

The critical ratio of the pore throat to the bacteria size was found to be 45 ~ `80 and 40 ~ 160 for LAS and Brijs, respectively. This is significantly larger than that observed in laboratory condition without surfactant which is 1.5. It means the threshold of occurrence of size exclusion was greatly decreased by surfactants, which is consistent with the fact that surfactants enhance the size exclusion effect.

5.2. Future work

The modeling of surfactant-enhanced bacteria transport through variably saturated media is not an extensively explored field. Although the model developed in this study successfully interpreted bacteria transport under the effect of various types and concentration. It still leaves room for improvement.

5.2.1. Bacteria Concentration Profile

One flaw of surfactant-enhanced bacteria transport model in this study is that the model is not calibrated with the bacteria concentration profile in the sand column and it operates the colloid deposition in a very simple way. The PI's experiment was not designed to measure the bacteria concentration along the sand column depth. Hence, there is no bacteria concentration profile to improve the reliability of the model. The concentration profile is also essential for exploring the deposition mechanisms in the porous media. Given the information gap, all physical and chemical processes affecting bacteria deposition were simply lumped in the first order deposition coefficient k in this study. And it cannot provide information to determine the primary deposition mechanism. Hence, future surfactant-enhanced bacteria transport should include a measurement of the bacteria concentration profile along the sand column. It would reinforce model validity and provide insight into deposition mechanisms.

5.2.2. Saturation Influence

The model does not elucidate the saturation influence even though it shows perfect application on bacteria transport in a variably saturated sand column. Because the water flow was constantly steady and the saturation distribution remained the same in the sand column throughout all experiments. The bacteria transport parameters in the model are

independent of saturation. However, saturation has significant impact on bacteria transport in porous media in that it greatly changes flow pattern in the porous media. Also, the air-water interface plays a key role in bacteria attachment. Further study involving bacteria transport within porous media under several uniform saturations is needed to reveal the saturation influence.

5.2.3. Applicable Model

At this stage, the model is more mechanical than applicable. Because the data on which the model is based is limited, it cannot be directly used in complex real-world problems. Even though several types of surfactant were investigated in this study, they only represent a small portion of surfactant products. Furthermore, only one type of bacteria and sand was used. A change in even one of these factors could result in different bacteria transport feature. Further research on surfactant-enhanced bacteria transport should involve more types and combinations of surfactants, bacteria, and sand to produce a model applicable in a variety of situations.

Appendix A. Derivation of Surfactant-Enhanced Bacteria Transport Model

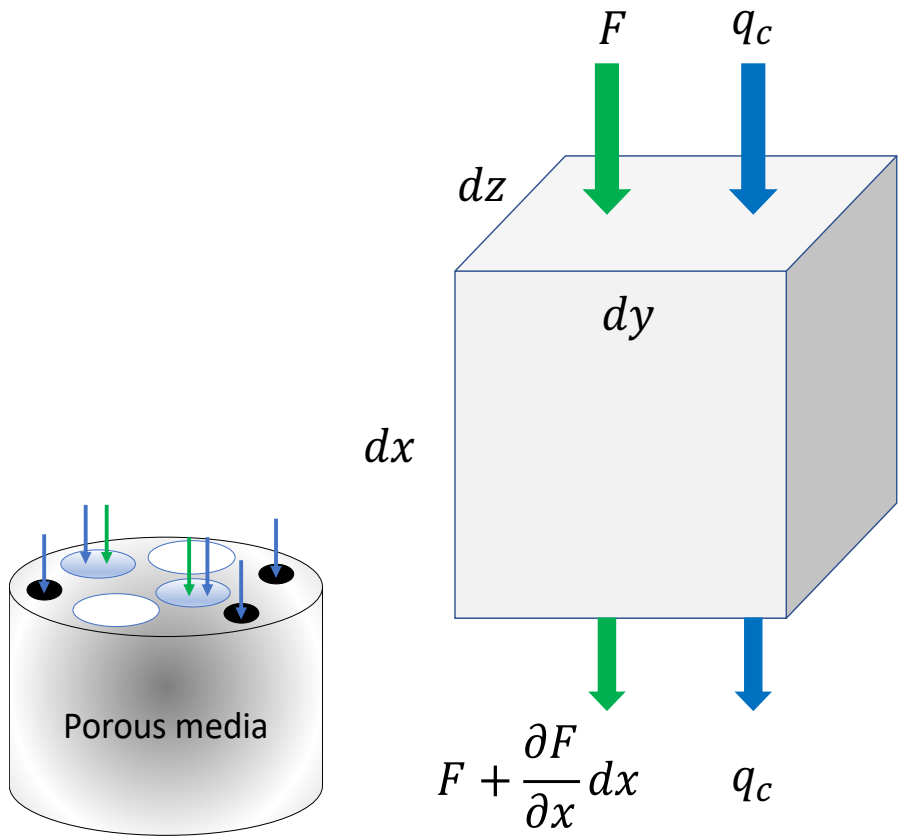

Figure A-1 Model of bacteria transport in porous media

The cubic in the figure represent a control volume in bacteria accessible region. F is mass (number) flux of bacteria per unit area per unit time [$NL^{-2}T^{-1}$]; qc is the bacteria accessible water velocity. Derivation started with mass balance analysis on control volume.

Mass balance in bacteria accessible region control volume:

$$\frac{d(mass)}{dt} = \{advection\} + \{dispersion\} + \{sorption\}$$

The bacteria entering the accessible region in the control volume due to {advection} [NT^{-1}] is expressed as:

$$\{advection\}_{in} = q_c c dydz \ .$$

The bacteria entering the accessible region in the control volume due to {dispersion} [NT^{-1}] is expressed by Fick's law:

$$\{dispersion\}_{in} = -\theta_c D \frac{\partial c}{\partial x} dydz$$

The total mass (number) of bacteria entering the accessible control volume [NT^{-1}] due to advection-dispersion effect is:

$$Fdydz = \{advection\}_{in} + \{dispersion\}_{in} = q_c c dydz - \theta_c D \frac{\partial c}{\partial x} dydz$$

Hence, we obtained the expression of F:

$$F = q_c c - \theta_c D \frac{\partial c}{\partial x}$$

The bacteria mass (number) flux [NT^{-1}] leaving the accessible control volume due to advection-dispersion effect is:

$$\{advection\}_{out} + \{dispersion\}_{out} = \left(F + \frac{\partial F}{\partial x} dx \right) dydz$$

The net bacteria mass (number) flux [NT^{-1}]:

$$\{advection\}_{net} + \{dispersion\}_{net} = Fdydz - \left(F + \frac{\partial F}{\partial x} dx \right) dydz = -\frac{\partial F}{\partial x} dxdydz$$

The mass loss due to {sorption} onto interfaces (SWI and GWI) [NT^{-1}]:

$$-\left(\rho_b \frac{\partial s}{\partial t} + A\frac{\partial \Gamma}{\partial t}\right) dxdydz$$

Where ρb is the bulk density [ML^{-3}]; s is bacteria concentration adsorbed to the solid phase [NM^{-1}]; A is air volume per unit porous media volume [L^3L^{-3}]; Γ is bacteria concentration adsorbed to the air phase [NL^{-3}].

Assuming first order kinetic irreversible sorption. Apply classical colloid theory approach, he accumulation of bacteria mass (number) on SWI and AWI is calculated as [$NL^{-3}T^{-1}$]:

$$\rho_b \frac{\partial s}{\partial t} = \theta_c k_1 c$$

$$A\frac{\partial \Gamma}{\partial t} = \theta_c k_2 c$$

Hence, the total sorbed bacteria mass [NT^{-1}] is:

$$\{sorption\} = -\left(\theta_c k_1 c + \theta_c k_2 c\right) dxdydz$$

Set k=k1+k2, lump sorption together [NT^{-1}]:

$$\{sorption\} = -\theta_c kcdxdydz$$

The bacteria mass change in the control volume over time [NT^{-1}] is:

$$\frac{\partial\left(c\theta_c dxdydz\right)}{dt}$$

Rewrite mass balance equation

$$\frac{\partial\left(c\theta_c dxdydz\right)}{dt} = -\frac{\partial F}{\partial x} dxdydz - \theta_c kcdxdydz$$

=>

$$\frac{\partial(c\theta_c)}{dt} = -\frac{\partial}{\partial x}\left(q_c c - \theta_c D\frac{\partial c}{\partial x}\right) - \theta_c kc$$

=>

$$\frac{\partial(c\theta_c)}{dt} + \theta_c kc = \frac{\partial}{\partial x}\left(\theta_c D\frac{\partial c}{\partial x}\right) - \frac{\partial(q_c c)}{\partial x}$$

Appendix B. Derivation of Pore Size Distribution

Equation of capillary rise height (h) [length] is expressed as:

$$h = \frac{2\sigma\cos(\alpha_c)}{\rho g r}$$

By adding a negative sign, this equation can be used to determine the largest pore radius (r) water fills at capillary pressure head (h):

$$h = -\frac{2\sigma\cos(\alpha_c)}{\rho g r}$$

This equation relates pore radius (r) to capillary pressure head (h).

van Genuchten (1980a) water retention function describes relationship between water content (θ) and capillary pressure head (h). It is expressed as:

Error! Objects cannot be created from editing field codes.

By replacing h with function of r, we obtained cumulative pore size distribution function. It determines the sum of relative water volume in the pores with radius not greater than r. It is assumed these pores are filled with water, so the relative water content is equal to relative pore space. The function θ(r) is expressed as:

$$\theta(r) = (\theta_s - \theta_r)\left\{1 + \left[2\sigma\cos(\alpha_c)\right]^n r^{-n}\right\}^{-m} + \theta_r$$

To obtain pore size distribution is simply the derivative of θ(r)

$$f(r) = \frac{d\theta}{dr}$$

$$= \frac{d(\theta_s - \theta_r)\left\{1 + \left[2\sigma\cos(\alpha_c)\right]^n r^{-n}\right\}^{-m} + \theta_r}{dr}$$

$$= \left(\theta_s - \theta_r\right)\left(-m\right)\left\{1+\left[2\sigma\cos\left(\alpha_c\right)\right]^n r^{-n}\right\}^{-m-1}\left[2\sigma\cos\left(\alpha_c\right)\right]^n\left(-n\right)r^{-n-1}$$

Rearrange:

$$f = mn\left(\theta_s - \theta_r\right)\frac{\left[2\sigma\cos\left(\alpha_c\right)\right]^n}{r^{n+1}+\left[2\sigma\cos\left(\alpha_c\right)\right]^n r}$$

References

[1] L. W. Canter, R. C. Knox, L. W. Canter, and L. W. Canter, *Evaluation of septic tank system effects on ground water quality*. US Environmental Protection Agency, Robert S. Kerr Environmental Research Laboratory, 1984.

[2] I. J. Buerge, H.-R. Buser, M. Kahle, M. D. Müller, and T. Poiger, "Ubiquitous Occurrence of the Artificial Sweetener Acesulfame in the Aquatic Environment: An Ideal Chemical Marker of Domestic Wastewater in Groundwater," *Environ. Sci. Technol.*, vol. 43, no. 12, pp. 4381–4385, Jun. 2009.

[3] M. V. Yates, "Septic Tank Density and Ground-Water Contamination," *Ground Water*, vol. 23, no. 5, pp. 586–591, Sep. 1985.

[4] M. J. Rosen and J. T. Kunjappu, *Surfactants and interfacial phenomena*. John Wiley & Sons, 2012.

[5] D. Myers, *Surfactant science and technology*. John Wiley & Sons, 2005.

[6] D. Rust and S. Wildes, "Surfactants: a market opportunity study update," *OmniTech Int. Ltd Midl. MI*, 2008.

[7] D. Arthur, "Little, Inc.(1991): Environmental and human safety of major surfactants. Arthur D. Little," *Inc Mass.*

[8] G. Bai, M. L. Brusseau, and R. M. Miller, "Influence of a Rhamnolipid Biosurfactant on the Transport of Bacteria through a Sandy Soil.," *Appl. Environ. Microbiol.*, vol. 63, no. 5, pp. 1866–1873, 1997.

[9] D. G. Brown and P. R. Jaffé, "Effects of Nonionic Surfactants on Bacterial Transport through Porous Media," *Environ. Sci. Technol.*, vol. 35, no. 19, pp. 3877–3883, Oct. 2001.

[10] G. Chen and H. Zhu, "Bacterial deposition in porous medium as impacted by solution chemistry," *Res. Microbiol.*, vol. 155, no. 6, pp. 467–474, 2004.

[11] M. J. Gross and B. E. Logan, "Influence of different chemical treatments on transport of Alcaligenes paradoxus in porous media.," *Appl. Environ. Microbiol.*, vol. 61, no. 5, pp. 1750–1756, 1995.

[12] A. Jackson, D. Roy, and G. Breitenbeck, "Transport of a bacterial suspension through a soil matrix using water and an anionic surfactant," *Water Res.*, vol. 28, no. 4, pp. 943–949, 1994.

[13] W. P. Johnson, M. J. Martin, M. J. Gross, and B. E. Logan, "Facilitation of bacterial transport through porous media by changes in solution and surface properties," *Colloids Surf. Physicochem. Eng. Asp.*, vol. 107, pp. 263–271, 1996.

[14] Q. Li and B. E. Logan, "Enhancing bacterial transport for bioaugmentation of aquifers using low ionic strength solutions and surfactants," *Water Res.*, vol. 33, no. 4, pp. 1090–1100, Mar. 1999.

[15] D. K. Powelson and A. L. Mills, "Water saturation and surfactant effects on bacterial transport in sand columns.," *Soil Sci.*, vol. 163, no. 9, pp. 694–704, 1998.

[16] M. L. Rockhold, R. R. Yarwood, M. R. Niemet, P. J. Bottomley, and J. S. Selker, "Experimental Observations and Numerical Modeling of Coupled Microbial and Transport Processes in Variably Saturated Sand," *Vadose Zone J.*, vol. 4, no. 2, pp. 407–417, May 2005.

[17] S. Sirivithayapakorn and A. Keller, “Transport of colloids in saturated porous media: A pore-scale observation of the size exclusion effect and colloid acceleration,” *Water Resour. Res.*, vol. 39, no. 4, p. 1109, Apr. 2003.
[18] S. H. Streger, S. Vainberg, H. Dong, and P. B. Hatzinger, “Enhancing Transport of Hydrogenophaga flava ENV735 for Bioaugmentation of Aquifers Contaminated with Methyl tert-Butyl Ether,” *Appl. Environ. Microbiol.*, vol. 68, no. 11, pp. 5571–5579, Nov. 2002.
[19] S. A. Bradford, J. Simunek, M. Bettahar, M. T. van Genuchten, and S. R. Yates, “Significance of straining in colloid deposition: Evidence and implications,” *Water Resour. Res.*, vol. 42, no. 12, p. W12S15, Dec. 2006.
[20] S. A. Bradford, J. Simunek, M. Bettahar, M. T. van Genuchten, and S. R. Yates, “Modeling Colloid Attachment, Straining, and Exclusion in Saturated Porous Media,” *Environ. Sci. Technol.*, vol. 37, no. 10, pp. 2242–2250, May 2003.
[21] T. R. Ginn, B. D. Wood, K. E. Nelson, T. D. Scheibe, E. M. Murphy, and T. P. Clement, “Processes in microbial transport in the natural subsurface,” *Adv. Water Resour.*, vol. 25, no. 8–12, pp. 1017–1042, Aug. 2002.
[22] T. R. Ginn, “A Brief Review of Bacterial Transport in Natural Porous Media,” Pacific Northwest Lab., Richland, WA (United States), PNL--10876, Dec. 1995.
[23] S. A. Bradford, J. Simunek, and S. L. Walker, “Transport and straining of E. coli O157:H7 in saturated porous media,” *Water Resour. Res.*, vol. 42, no. 12, p. W12S12, Dec. 2006.
[24] J. Šimůnek, C. He, L. Pang, and S. A. Bradford, “Colloid-Facilitated Solute Transport in Variably Saturated Porous Media,” *Vadose Zone J.*, vol. 5, no. 3, pp. 1035–1047, Aug. 2006.
[25] M. Y. Corapcioglu and H. Choi, “Modeling Colloid Transport in Unsaturated Porous Media and Validation with Laboratory Column Data,” *Water Resour. Res.*, vol. 32, no. 12, pp. 3437–3449, Dec. 1996.
[26] J. Wan and J. L. Wilson, “Colloid transport in unsaturated porous media,” *Water Resour. Res.*, vol. 30, no. 4, pp. 857–864, Apr. 1994.
[27] A. Schäfer, P. Ustohal, H. Harms, F. Stauffer, T. Dracos, and A. J. B. Zehnder, “Transport of bacteria in unsaturated porous media,” *J. Contam. Hydrol.*, vol. 33, no. 1–2, pp. 149–169, Sep. 1998.
[28] D. G. Brown and P. R. Jaffé, “Effects of Nonionic Surfactants on Bacterial Transport through Porous Media,” *Environ. Sci. Technol.*, vol. 35, no. 19, pp. 3877–3883, Oct. 2001.
[29] D. G. Brown and P. R. Jaffé, “Effects of Nonionic Surfactants on the Cell Surface Hydrophobicity and Apparent Hamaker Constant of a Sphingomonas sp,” *Environ. Sci. Technol.*, vol. 40, no. 1, pp. 195–201, Jan. 2006.
[30] H. Kim, K.-M. Choi, J.-W. Moon, and M. D. Annable, “Changes in air saturation and air–water interfacial area during surfactant-enhanced air sparging in saturated sand,” *J. Contam. Hydrol.*, vol. 88, no. 1–2, pp. 23–35, Nov. 2006.
[31] E. J. Henry, J. E. Smith, and A. W. Warrick, “Surfactant effects on unsaturated flow in porous media with hysteresis: horizontal column experiments and numerical modeling,” *J. Hydrol.*, vol. 245, no. 1–4, pp. 73–88, May 2001.
[32] E. J. Henry, J. E. Smith, and A. W. Warrick, “Solubility effects on surfactant-induced unsaturated flow through porous media,” *J. Hydrol.*, vol. 223, no. 3–4, pp. 164–174, Oct. 1999.

[33] W. B. Mills, S. Liu, and F. K. Fong, “Literature Review and Model (COMET) for Colloid/Metals Transport in Porous Media,” *Ground Water*, vol. 29, no. 2, pp. 199–208, Mar. 1991.
[34] J. Šimůnek, M. Šejna, and M. T. van Genuchten, “The C-Ride Module for HYDRUS (2D/3D) Simulating two-dimensional colloid-facilitated solute transport in variably-saturated porous media,” *PC Prog. Prague Czech Repub.*, p. 45, 2012.
[35] J. Simunek, K. Huang, M. Sejna, M. van (Salinity L. Genuchten, V. Novak, and J. (Slovak A. of S. Sutor, “The HYDRUS-ET software package for simulating the one-dimensional movement of water, heat, and multiple solutes in variably-saturated media. Version 1.1,” 1997. .
[36] J. Simunek, D. Jacques, G. Langergraber, S. A. Bradford, M. Šejna, and M. T. van Genuchten, “Numerical Modeling of Contaminant Transport Using HYDRUS and its Specialized Modules,” *J. Indian Inst. Sci.*, vol. 93, no. 2, pp. 265–284, Jun. 2013.
[37] J. N. Ryan and M. Elimelech, “Colloid mobilization and transport in groundwater,” *Colloids Surf. Physicochem. Eng. Asp.*, vol. 107, pp. 1–56, Feb. 1996.
[38] D. B. Stephens, *Vadose zone hydrology*. CRC press, 1995.
[39] R. A. Freeze and J. A. Cherry, *Groundwater, 604 pp*. Prentice-Hall, Englewood Cliffs, NJ, 1979.
[40] D. E. Radcliffe and J. Simunek, *Soil physics with HYDRUS: Modeling and applications*. CRC Press/Taylor & Francis, 2010.
[41] F. A. Dullien, *Porous media: fluid transport and pore structure*. Academic press, 2012.
[42] J. C. van Dam and R. A. Feddes, “Numerical simulation of infiltration, evaporation and shallow groundwater levels with the Richards equation,” *J. Hydrol.*, vol. 233, no. 1, pp. 72–85, Jun. 2000.
[43] J. H. Dane and R. J. Lenhard, “HYSTERESIS,” *Encycl. Soils Environ. Four-Vol. Set*, pp. 231–237, 2005.
[44] M. T. van Genuchten, “A Closed-form Equation for Predicting the Hydraulic Conductivity of Unsaturated Soils1,” *Soil Sci. Soc. Am. J.*, vol. 44, no. 5, p. 892, 1980.
[45] J. Šimůnek and J. W. Hopmans, “1.7 Parameter Optimization and Nonlinear Fitting,” *Methods Soil Anal. Part 4 Phys. Methods*, no. methodsofsoilan4, pp. 139–157, 2002.
[46] F. W. Schwartz and H. Zhang, “Fundamentals of Groundwater John Wiley & Sons,” *N. Y.*, vol. 583, 2003.
[47] W. R. Gardner, “Some steady-state solutions of the unsaturated moisture flow equation with application to evaporation from a water table.,” *Soil Sci.*, vol. 85, no. 4, pp. 228–232, 1958.
[48] G. S. Campbell, “A simple method for determining unsaturated conductivity from moisture retention data.,” *Soil Sci.*, vol. 117, no. 6, pp. 311–314, 1974.
[49] R. Haverkamp, M. Vauclin, J. Touma, P. J. Wierenga, and G. Vachaud, “A comparison of numerical simulation models for one-dimensional infiltration,” *Soil Sci. Soc. Am. J.*, vol. 41, no. 2, pp. 285–294, 1977.
[50] N. Burdine, “Relative permeability calculations from pore size distribution data,” *J. Pet. Technol.*, vol. 5, no. 03, pp. 71–78, 1953.
[51] Y. Mualem, “A new model for predicting the hydraulic conductivity of unsaturated porous media,” *Water Resour. Res.*, vol. 12, no. 3, pp. 513–522, 1976.
[52] J. R. Nimmo, “Porosity and pore size distribution,” *Encycl. Soils Environ.*, vol. 3, pp. 295–303, 2004.

[53] A. Pedescoll, R. Samsó, E. Romero, J. Puigagut, and J. García, “Reliability, repeatability and accuracy of the falling head method for hydraulic conductivity measurements under laboratory conditions,” *Ecol. Eng.*, vol. 37, no. 5, pp. 754–757, May 2011.
[54] J. Stibinger, *Examples of Determining the Hydraulic Conductivity of Soils: Theory and Applications of Selected Basic Methods: University Handbook on Soil Hydraulics*. Jan Evangelista Purkyně University, Faculty of the Environment, 2014.
[55] A. E. Fryar, “Fundamentals of Ground Water (Franklin W. Schwartz and Hubao Zhang),” *Environ. Eng. Geosci.*, vol. 11, no. 3, pp. 285–286, Mar. 2005.
[56] D. Hillel, “Fundamentals of soil physics.,” p. 413pp., 1980.
[57] K. Kosugi, J. W. Hopmans, and J. H. Dane, “Methods of soil analysis. Part 4. Physical methods.,” *SSSA Book Ser.*, pp. 728–757, 2002.
[58] M. A. Celia, E. T. Bouloutas, and R. L. Zarba, “A general mass-conservative numerical solution for the unsaturated flow equation,” *Water Resour. Res.*, vol. 26, no. 7, pp. 1483–1496, Jul. 1990.
[59] T. Vogel and M. Cislerova, “On the reliability of unsaturated hydraulic conductivity calculated from the moisture retention curve,” *Transp. Porous Media*, vol. 3, no. 1, pp. 1–15, 1988.
[60] J. C. Van Dam, J. N. M. Stricker, and P. Droogers, “Inverse method to determine soil hydraulic functions from multistep outflow experiments,” *Soil Sci. Soc. Am. J.*, vol. 58, no. 3, pp. 647–652, 1994.
[61] F. Abbasi, J. Simunek, J. Feyen, M. T. Van Genuchten, and P. J. Shouse, “Simultaneous inverse estimation of soil hydraulic and solute transport parameters from transient field experiments: Homogeneous soil,” *Trans. ASAE*, vol. 46, no. 4, p. 1085, 2003.
[62] J. Šimůnek, V. Genuchten, M. Th, and M. Šejna, “Development and Applications of the HYDRUS and STANMOD Software Packages and Related Codes,” *Vadose Zone J.*, vol. 7, no. 2, pp. 587–600, May 2008.
[63] C. R. Woese, O. Kandler, and M. L. Wheelis, “Towards a natural system of organisms: proposal for the domains Archaea, Bacteria, and Eucarya.,” *Proc. Natl. Acad. Sci. U. S. A.*, vol. 87, no. 12, pp. 4576–4579, Jun. 1990.
[64] W. B. Whitman, D. C. Coleman, and W. J. Wiebe, “Prokaryotes: the unseen majority,” *Proc. Natl. Acad. Sci.*, vol. 95, no. 12, pp. 6578–6583, 1998.
[65] R. W. Harvey and H. Harms, “Tracers in groundwater: use of microorganisms and microspheres,” *Encycl. Environ. Microbiol.*, 2002.
[66] Y. Jin and M. Flury, “Fate and transport of viruses in porous media,” in *Advances in agronomy*, vol. 77, Elsevier, 2002, pp. 39–102.
[67] G. Gargiulo, S. A. Bradford, J. Simunek, P. Ustohal, H. Vereecken, and E. Klumpp, “Bacteria transport and deposition under unsaturated flow conditions: The role of water content and bacteria surface hydrophobicity,” *Vadose Zone J.*, vol. 7, no. 2, pp. 406–419, 2008.
[68] M. Y. Corapcioglu and A. Haridas, “Transport and fate of microorganisms in porous media: a theoretical investigation,” *J. Hydrol.*, vol. 72, no. 1–2, pp. 149–169, 1984.
[69] S. W. Taylor and P. R. Jaffé, “Biofilm growth and the related changes in the physical properties of a porous medium: 3. Dispersivity and model verification,” *Water Resour. Res.*, vol. 26, no. 9, pp. 2171–2180, 1990.
[70] Y. Tan, J. T. Gannon, P. Baveye, and M. Alexander, “Transport of bacteria in an aquifer sand: Experiments and model simulations,” *Water Resour. Res.*, vol. 30, no. 12, pp. 3243–3252, Dec. 1994.

[71] H. Yuan and A. A. Shapiro, “Colloid transport and retention: recent advances in colloids filtration theory,” *Colloids Classif. Prop. Appl.*, pp. 201–242, 2012.
[72] S. A. Bradford and S. Torkzaban, “Colloid Transport and Retention in Unsaturated Porous Media: A Review of Interface-, Collector-, and Pore-Scale Processes and Models,” *Vadose Zone J.*, vol. 7, no. 2, pp. 667–681, May 2008.
[73] S. Niehren and W. Kinzelbach, “Artificial colloid tracer tests: development of a compact on-line microsphere counter and application to soil column experiments,” *J. Contam. Hydrol.*, vol. 35, no. 1–3, pp. 249–259, 1998.
[74] D. R. Champ and J. Schroeter, “Bacterial transport in fractured rock–A field-scale tracer test at the Chalk River Nuclear Laboratories,” *Water Sci. Technol.*, vol. 20, no. 11–12, pp. 81–87, 1988.
[75] L. M. McDowell-Boyer, J. R. Hunt, and N. Sitar, “Particle transport through porous media,” *Water Resour. Res.*, vol. 22, no. 13, pp. 1901–1921, 1986.
[76] H. E. Kubitschek, “Cell volume increase in Escherichia coli after shifts to richer media.,” *J. Bacteriol.*, vol. 172, no. 1, pp. 94–101, Jan. 1990.
[77] N. M. DeNovio, J. E. Saiers, and J. N. Ryan, “Colloid Movement in Unsaturated Porous Media,” *Vadose Zone J.*, vol. 3, no. 2, pp. 338–351, May 2004.
[78] J. G. Kirkwood, R. L. Baldwin, P. J. Dunlop, L. J. Gosting, and G. Kegeles, “Flow equations and frames of reference for isothermal diffusion in liquids,” *J. Chem. Phys.*, vol. 33, no. 5, pp. 1505–1513, 1960.
[79] J. Philibert, “One and a half century of diffusion: Fick, Einstein, before and beyond,” *Diffus. Fundam.*, vol. 2, no. 1, pp. 1–10, 2005.
[80] N. Tufenkji and M. Elimelech, “Deviation from the classical colloid filtration theory in the presence of repulsive DLVO interactions,” *Langmuir*, vol. 20, no. 25, pp. 10818–10828, 2004.
[81] K. E. Nelson and T. R. Ginn, “Colloid filtration theory and the Happel sphere-in-cell model revisited with direct numerical simulation of colloids,” *Langmuir*, vol. 21, no. 6, pp. 2173–2184, 2005.
[82] P. R. Johnson, N. Sun, and M. Elimelech, “Colloid Transport in Geochemically Heterogeneous Porous Media: Modeling and Measurements,” *Environ. Sci. Technol.*, vol. 30, no. 11, pp. 3284–3293, Oct. 1996.
[83] D. W. Marquardt, “An algorithm for least-squares estimation of nonlinear parameters,” *J. Soc. Ind. Appl. Math.*, vol. 11, no. 2, pp. 431–441, 1963.
[84] B. S. Levy and R. M. Chambers, “Bromide as a conservative tracer for soil-water studies,” *Hydrol. Process.*, vol. 1, no. 4, pp. 385–389, Nov. 1987.
[85] M. Huysmans and A. Dassargues, “Review of the use of Péclet numbers to determine the relative importance of advection and diffusion in low permeability environments,” *Hydrogeol. J.*, vol. 13, no. 5–6, pp. 895–904, Oct. 2005.
[86] C. G. Enfield, G. Bengtsson, and R. Lindqvist, “Influence of macromolecules on chemical transport,” *Environ. Sci. Technol.*, vol. 23, no. 10, pp. 1278–1286, 1989.
[87] P. W. Reimus, “The use of synthetic colloids in tracer transport experiments in saturated rock fractures,” University of New Mexico Albuquerque, NM, 1995.
[88] D. K. Powelson, C. P. Gerba, and M. T. Yahya, “Virus transport and removal in wastewater during aquifer recharge,” *Water Res.*, vol. 27, no. 4, pp. 583–590, 1993.
[89] R. C. Bales, C. P. Gerba, G. H. Grondin, and S. L. Jensen, “Bacteriophage transport in sandy soil and fractured tuff,” *Appl. Environ. Microbiol.*, vol. 55, no. 8, pp. 2061–2067, 1989.

[90] C. V. Chrysikopoulos and A. Abdel-Salam, “Modeling colloid transport and deposition in saturated fractures,” *Colloids Surf. Physicochem. Eng. Asp.*, vol. 121, no. 2–3, pp. 189–202, 1997.
[91] H. Gvirtzman and S. M. Gorelick, “Dispersion and advection in unsaturated porous media enhanced by anion exclusion,” *Nature*, vol. 352, no. 6338, pp. 793–795, Aug. 1991.
[92] S. Srinivasan, *Fuel cells: from fundamentals to applications*. Springer Science & Business media, 2006.
[93] D. A. Horneman, M. Ottens, J. T. F. Keurentjes, and L. A. M. van der Wielen, “Surfactant-aided size-exclusion chromatography for the purification of immunoglobulin G,” *J. Chromatogr. A*, vol. 1157, no. 1–2, pp. 237–245, Jul. 2007.

Vita

Zhu Jialan

917-561-2547 | drewjialan@gmail.com | New York, NY 10018

Education

Ph.D.
Sep 2014 – May 2019
Water Resources Engineering
Doctoral dissertation: Surfactant-Enhanced Size-Excluded Transport of Bacteria in Unsaturated Porous Media

Master of Science
Sep 2011 – May 2014
Water Resources Engineering

Bachelor of Science
Sep 2007 – May 2011
Water Resources Engineering

Academic Employment

Teaching Assistant
Sep 2015 – Jan 2016
Department of Civil and Environmental Engineering
Responsibilities include: assisting professors with the preparation and presentation of undergraduate courses, tutoring recitation, grading, and leading demonstration labs.

Presentations at Professional Meetings

American Geophysical Union
Dec 2017
Poster Presentation: Surfactant-Enhanced Size-Excluded Transport of Bacteria in Unsaturated Porous Media

New England Graduate Student Water Symposium (NEGSWS)
Sep 2015
Poster Presentation: Bacteria Transport in Vadose Zone